A tuneable all solid state laser based on Cr^{4+}:YAG

Thesis submitted for the degree of Master of Science by thesis to the

University of St.Andrews

by

Robert M.L. Schnekenbühl

Department of Physics and Astronomy

University of St.Andrews

North Haugh

St.Andrews, Fife

Scotland. KY16 9SS

August 1992.

I Robert Schnekenbühl hereby certify that this thesis has been composed by myself, that it is a record of my own work, and that it has not been accepted in partial or complete fulfilment of any other degree or professional qualification.

St. Andrews, den 29.08.1992

I hereby certify that the candidate has fulfilled the conditions of the Resolution and Regulations appropriate to the Degree of M.Sc. by research.

Signature of Supervisor

St.Andrews, den 31.08.1992

Copyright

To the good old Royal Burgh of St. Andrews and my grand children.

Abstract

This thesis describes the development of a tuneable all-solid state cw-laser system producing radiation at wavelengths in the vicinity of $1.5\mu m$. The active medium was a $Cr^{4+}:YAG$. crystal which was pumped at $1064nm$ by a Nd:YAG laser. The $Cr^{4+}:YAG$ laser was operated in a symmetrical z-cavity configuration, and numerical calculations were carried out to design the resonator to have optimum astigmatic compensation. The performance of the laser was found to be in general agreement with theory. Under optimum circumstances it was found that the laser operated at over 10% conversion efficiency, producing typically $520mW$ average power, at $5.2W$ pump power, tuneable from $1360nm$ to $1530nm$.

In addition to the construction and characterisation of the laser in a cw configuration, preliminary experiments were carried out to investigate the mode-locked performance of the laser. Using an acousto-optic modulator in a regenerative mode-locked configuration, pulses of duration less than $45ps$ have been achieved. Some addition to the mode-locked laser system to achieve femtosecond pulses are also considered.

CONTENTS

page No

ABSTRACT I

CONTENTS II

ABREVATIONS III

1 Introduction 1

1.1 Solid State Lasers 1

1.2 References 4

2. Material Properties of Cr:YAG.....5

2.1 Energy Level Diagram.....5

2.2 Absorption Spectrum of Cr^{4+}:YAG 6

2.3 Fluorescence Spectrum of Cr^{4+}:YAG 8

2.4 Polarisation of the Cr^{4+}:YAG-Crystal in the Brewster-angled cut Rod.....9

2.5 Conclusions.....11

2.6 References 11

3. Cavity design.....12

3.1. Ray propagation.....12

3.2 Description of Optical Elements by Matrices.....13

3.2.1 Matrices describing Special Optical Elements 14

Non Astigmatic Elements 14

Astigmatic Elements 15

3.2.2 Combination of Different Elements by Ordered Multiplication of Matrices.....19

3.2.3 Sequences 19

3.2.4 Round-Trip-Matrix 21
3.3. Gaussian Beam 22
3.3.1 Gaussian Beam 22
3.3.2 ABCD-Law 24
3.4 Resonator 25
3.4.1 Optical Resonator Algebra 25
3.4.2 Astigmatic Gaussian Beam 27
3.4.3 Regions of stability 28
3.4.4 Astigmatic Compensation 28
Suitable Structure of the Cavity 28
3.4.5 Parameters 29
[a] Angle of the Folding Section 29
[b] Position of the Mirrors of the Folding Section 30
[c] Total Length of the Cavity 32
[d] Radius of Curvature 32
3.4.6 Radiation Volume inside the Crystal taken up by the Signal 33
3.5 Pump beam 34
3.5.1 Influence of the Pump Laser on the Efficiency of the System 35
3.5.2 Volume inside the Crystal taken up by the Pump beam 35
3.6 Conclusions 36
3.7 References 37

4. Experimental Characteristics of CW Laser Operation 39
4.1. Cavity Elements 39
4.1.1 Mounting of the Crystal 39
4.1.2 Pump Laser 41
4.1.3 Mirror sets 41

4.2. Cavity Stability Considerations....42
4.2.1 Numerical Computation....42
4.2.1.1 Dependence on ϑ....48
4.2.1.2 Dependence on d....52
4.2.1.3 Dependence on R....56
4.2.2 Experimental Results....58
4.4. Characterisation of Laser Oscillation....63
4.4.1 Output Power....64
4.4.2 Dependence on the Temperature....66
4.4.3 Optimum Output Coupling....67
4.4.4 Oscillation Frequency....69
4.4.5 Tuneability....70
4.5 Conclusions....73
4.6 References....73

5 Conclusion and Suggestions for Further Study....75
5.1 Conclusions....75
5.2 Preliminary Mode-locking Results....75
5.3 Suggestions for Further Studies....76
5.4 References....76

ACKNOLEDGMENTS 77

Abbreviations used in this thesis

BRF	birefringent filter
c	velocity of light in vacuum
cc	colour centre
d	total length of the cavity
d_1	length of the leg of the cavity + δ
δ	relative adjustment of the mirrors in the folding section of the z-shape cavity
δ^*	optimum δ in respect to maximising Ω
d_{rod}	geometrical length of the rod
Δ	distance of the pre-focal lens to the crystal
$\underline{e_k}$	eigenvector
E_2	identity matrix $\in M_2$
$E(z)$	field amplitude
f	focal length of the pre-focal lens
Γ	overlap of S_t and S_s
L	total loss within a cavity
L_i	inevitable losses of a cavity
λ	wavelength
λ_k	eigenvalue
M_i	matrices $\in M_2$
M_R	round-trip matrix $\in SO_2$
n	refractive index
q	complex beam parameter
r	reflectivity of an optical element

R	radius of curvature of mirror for the folding section
S_s	range of stability as a function of δ in the sagittal plane
S_t	range of stability as a function of δ in the tangential plane
SO_2	special orthogonal group in the 2-dimensional vector space over the real figures
t	thickness of the crystal out of which the rod is cut
T	Transmission of an output coupler
T_{opt}	optimum transmission of the out coupling element
$T_{\max}$	Maximum transmission where the total loss L is equal to the gain
ϑ	angle of the off axis mirror
ϑ^*	optimum astigmatic compensation angle
Ω	product of $\omega_s \omega_t$
ω_0	beamwaist
ω_s	spotsize in the sagittal plane
ω_s^*	ω_s at δ^*
ω_t	spotsize in the tangential plane
ω_t^*	ω_t at δ^*
V	volume taken up by the beam inside the crystal
YAG	$Y_3Al_5O_{12}$

1 Introduction

1.1 Solid State Lasers

The active media of solid state lasers consist of crystals or glass-hosts which are doped with active ions. The most common ions are ions of the transition metals or the rare earth elements. The laser transition takes place between the inner free shells which are not disturbed by the field of the host. This results in narrow transitions and effects the small signal gain and therefore the threshold of the pump positively. The doping with host-ions is mostly not higher than 1% by weight. Nevertheless the density of active ions is of the order of $10^{19} cm^{-3}$. This is higher than for instance in a gas laser ($10^{15} - 10^{17} cm^{-3}$). In spite of the relatively small efficiency of typically up to 1%, solid state lasers achieve high output power. Excitation usually is achieved by optical pumping by arclight, other lasers or recently by diode arrays.

Some common solid state lasers operating at room temperature are the lasers based on the following materials: ruby[1], Nd:YAG, Nd:Glass, Ti:Sapphire, Alexandrite, Emerald, Cr:GSAG, Cr:GSGG, Cr:$KZnF_3$, Cr:$SrAlF_5$, Cr^{4+}:*YAG* and others. In addition to these lasers there are a large class of solid state lasers which require cryogenic cooling to liquid nitrogen temperature. These are the Cr:$ZnWO_4$, Co:MgF_2, Ni:MgF_2, Co:$KZnF_3$, the colour centre lasers and others. Solid state lasers operating on purely electronic transitions tend to be narrow bandwidth sources for instance Nd:YAG and the ruby-laser; many other solid state lasers operate on vibronic transition which results in broad tuneability over wide range. For the range in which some of these lasers can be tuned see figure 1.1.

The application of such systems in continuous wave (cw)-operation are in the field of spectroscopy. Pulsed solid state lasers are used for a variety of smaller-scale laser

cutting[2], drilling[3], and marking applications; as geodesically, meteorological and military range finders and target designators[4]; medical applications especially in the ophthalmology[5]; and in an enormous variety of scientific and technological experiments; in particular time resolved spectroscopy where the dynamical behaviour of chemical and biological processes is studied.

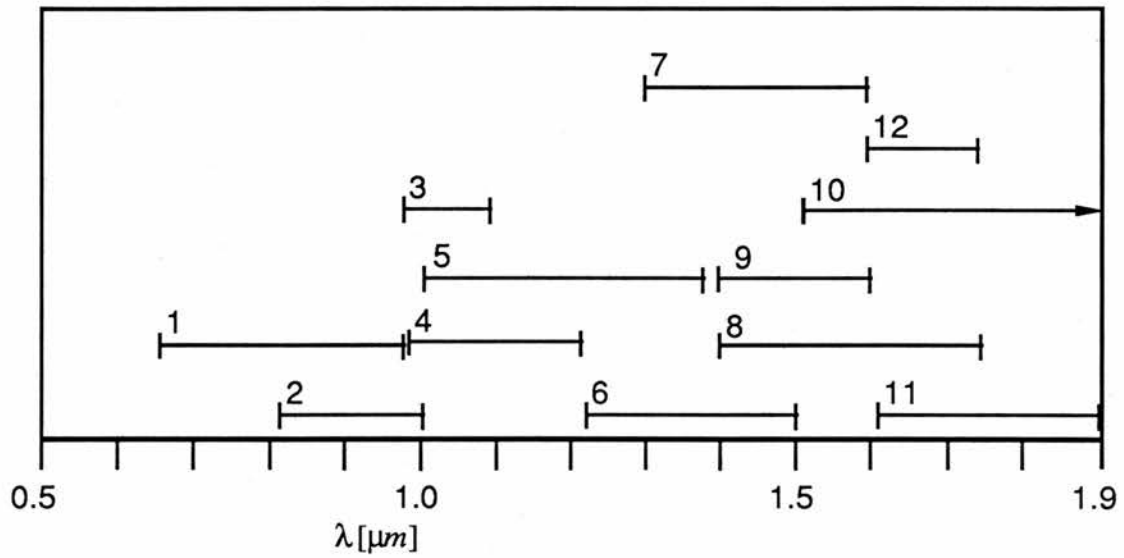

Figure 1. : Diagram showing some solid state lasers and their tuning ranges[6]: (1) Ti:Saphire, (2) LiF, (3) Cr:$ZnWO_4$, (4) NaF $(F_2^+)^*$, (5) NaF $(F_2^+)^{**}$, (6) KF, (7) Cr4+:YAG, (8) NaCl, (9) KCl:Tl, (10) Co:MgF_2, (11) KCl:Na and (12) Ni:MgF_2.

Tuneable solid state lasers have applicability where their advantages - tuneability, high storage of energy and high average power - can be useful. These are the fields of photo chemistry[7], LIDAR (light detecting and ranging) in its various features for atmospheric examinations[8], non linear optics[9] and the separation of ions[10].

Another important application of solid state lasers is their ability to provide light at wavelengths of $1.3\mu m$ to $1.5\mu m$. This is needed for studies of the properties of optical fibres. For applicability in optical fibres the dispersion losses have to be considered as well as the dispersive spreading in the material. In typical fibres the net dispersion passes

through zero at a wavelength around 1.3μm, so that in principle very short pulses tuned to this wavelength could be propagated for very long distances without dispersive spreading. The lowest loss wavelength for optical fibres is typically closer to 1.5μm (at which wavelength the absorption and scattering losses in real fibres can have values down to $\approx 0.2\text{dB/km}$). It is therefore desirable to employ a laser which can be tuned to this wavelength.

This thesis discusses the develop of a tuneable cw-laser source based on Cr^{4+}:YAG. It is important to consider its specific advantages over other lasers mentioned.

Its operating wavelength is 1450nm which is ideal for study of optical fibre properties. The only other high power source at this wavelength is the colour centre laser which has many disadvantages. The colour centre crystals are fragile, requiring constant cryogenic cooling and protection from all sources of UV light. By contrast the Cr^{4+}:YAG operates at room temperature and only requires tap water cooling to about 8 to 18C^o. This fact does not only render superfluous the more complicated astigmatic compensation due to the additional windows of the cryostat in which the cc-crystals are situated but also has advantages in economical aspects and its more convenient technical applicability.

The Cr^{4+}:YAG -laser is tuneable from 1300nm up to 1600nm[11]. This laser therefore provides an attractive alternative to the cc-lasers for production of radiation @1.5μm.

This thesis discusses material properties of the Cr^{4+}:YAG crystal in chapter 2, and considers why it is such a useful source. It then outlines the essential theory of cavity design in chapter 3 and applies this to the design of a resonator to provide stable, efficient and tuneable cw-lasing operation in chapter 4. In chapter 5 a brief discussion of the possibilities of mode locked operation will be given.

1.2 References

1 Maiman, T.H.: *Nature*, vol.187, p.493, **1960**

2 Beyer, E. & al.: *Laser und Optoelektronik* vol.3, p.282, **1985**

3 Treusch & al.: *Laser und Optoelektronik* vol.4, p.397, **1985**

4 Köchner, W.:Solid-State Laser Engineering, Springer Series in Optical Science, vol.1, Berlin, **1988**

5 Schröder, E.: *Laser und Optoelektronik*, vol.3, p.209, **1983**

6 Mollenauer, L.F.: "Color Center Lasers" (chapter 2), in Laser Handbook, vol.4, Stich and Bass, eds.Amsterdam, **1985**; Walling, J.C.: Tunable Lasers, (ed. L.F. Mollenauer & J.C.White), Topics i n Applied Physics, vol.59, chapter 9, Berlin **1987;** Kneubühl, F.K. & Sigrist, M.W.: Laser Stuttgart **1991**

7 West, G.A. & al.: *J. Chem. Phys.* vol.75, p.2006, **1981**

8 Roulard III, F.R.: Tunable Solid State Lasers (ed. P. Hammerling, A.B. Budgor, A. Pinto) Springer Series in Optical Sciences vol.47, p.35, Berlin **1985**

9 Shen, Y.R.: The Principles of Nonlinear Optics New York **1984**

10 Sam & al.: Tunable Solid State Lasers, (ed. P. Hammerling, A.B. Budgor, A. Pinto), Springer Series in Optical Sciences vol. 47, p.28, Berlin **1985**

11 Shestakov A.V. & al.: Tunable Cr^{4+}:*YAG* Lasers, *Conference on Lasers and Electro Optics,* CLEO Baltimore, Marryland, May 12-17 **1991**, Postdeadline-papers

2. Material Properties of Cr:YAG

The crystal used was a Cr^{4+}:*YAG* Czochralski grown rod manufactured in Russia. The crystal properties discussed here were examined by the Russian manufacturers. Other Institutes (for example: Institut für Laser-Physik, Hamburg) are at the moment concerned with further studies of these material properties. The first work with this crystal used as a promising material for a solid state laser emitting light in the region of 1300*nm* to 1600*nm* was mainly motivated by a post-deadline paper for CLEO 1991 by Shestakov[1] . The following details were either provided by the first examination of the Cr^{4+}:*YAG* by Borodin and Shestakov or by our own measurements of the fluorescence and absorption spectrum in the J.F.Allen Research Laboratories in St.Andrews. These measurements were carried out with a Brewster-angled cut cylindrical rod of 26*mm* with a diameter of about 5*mm*. Because of the Brewster cut nature of the rod, a detailed investigation of the spectral properties of the crystal by methods of polarisation spectroscopy was not possible-indeed a discussion of these properties is beyond the scope of this thesis. The following chapter will therefore only discuss the most obvious properties of the crystal as they relate to choice of an appropriate pump laser and the expected emitted laser wavelength.

2.1 Energy Level Diagram

In order to analyse the oscillation characteristics, a five-level scheme for the operation levels of the active medium has been used (figure 2.1). This scheme corresponds to Cr^{4+}-ions situated in a distorted tetrahedral field with local symmetry D_{2d} which is to be found in YAG crystals. The values of the parameters in this scheme are as follows: the absorption cross sections at the pumping wavelength from the main and excited states are

given by $\sigma_1 = 5[\pm 1]10^{-18} cm^2$ and $\sigma_2 = 5[\pm 2]10^{-19} cm^2$ respectively with corresponding excitation relaxation times $\tau_1 = 4 \cdot 10^{-6} s$ and $\tau_2 = 10^{-10} s$.

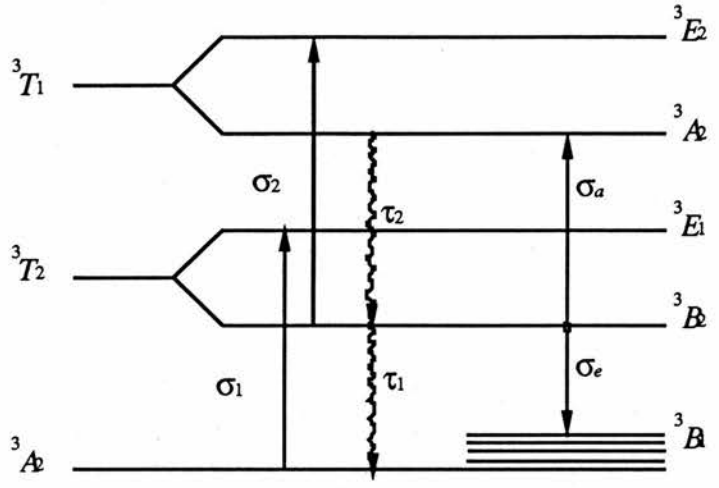

Figure 2.1 : Energy level diagram of Cr^{4+} site in disordered tetrahedral field with the local symmetry of D2d after [Shestakov 1991][2].

The cross section of the emission is given by $\sigma_e = 7 - 8 \cdot 10^{-19} cm^2$. There also exists a self absorption which is characterised by the absorption cross section of $\sigma_a = 4 - 5 \cdot 10^{-19} cm^2$. These values have been found experimentally by Borodin and Shestakov.

2.2 Absorption Spectrum of Cr^{4+}:YAG

The absorption spectrum of the given crystal was measured using a monochrometer together with a white light source. The transmission spectrum of the rod and the spectrum of the lamp were taken separately and the absorption spectrum was obtained by dividing these two spectra using the computer attached to the system. The result is shown in figure 2.2[a]. Note the band of absorption between 950*nm* and 1100*nm* which enables the material to be pumped by a Nd:YAG laser at 1064.1*nm*. There is also no significant absorption in the region of 1300*nm* to 1600*nm*. This is important to note as significant

absorption in this region would introduce more inevitable loss of a laser emitting between 1300*nm* and 1600*nm* due to self absorption. A detail of this absorption spectrum is shown in figure 2.2[b]. The maximum of the absorption band is at 1030*nm*. At 1060*nm* the absorption is on 80% of its maximum.

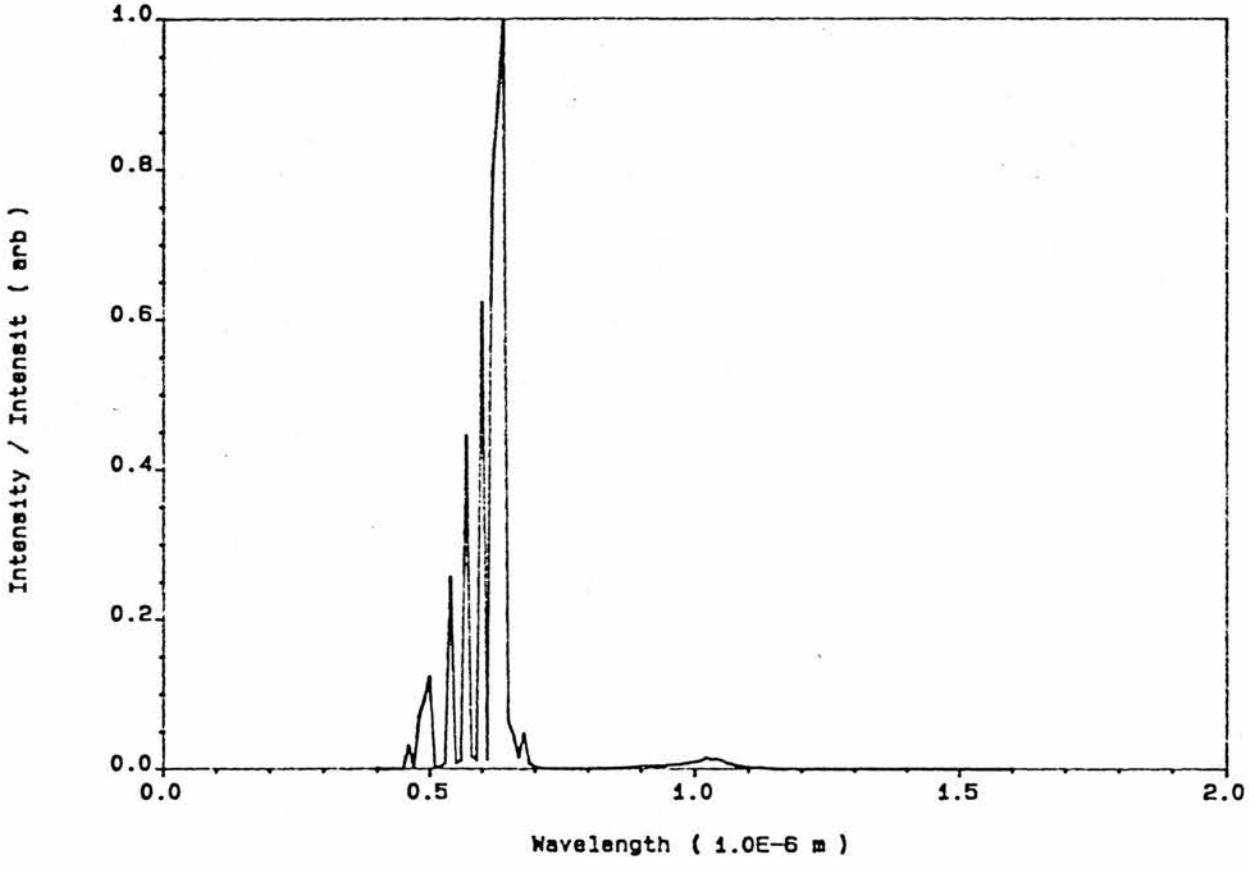

Figure 2.2 [a] : Absorption spectrum of Cr^{4+}:*YAG*.

Notice that the absorption spectrum here consists of a series of narrow bands. This arises because the transitions in Cr^{4+}:*YAG* are mainly electronic in nature, and is in contrast with the broad band absorption seen in laser materials such as Ti:Sapphire where the transitions are mainly vibronic.

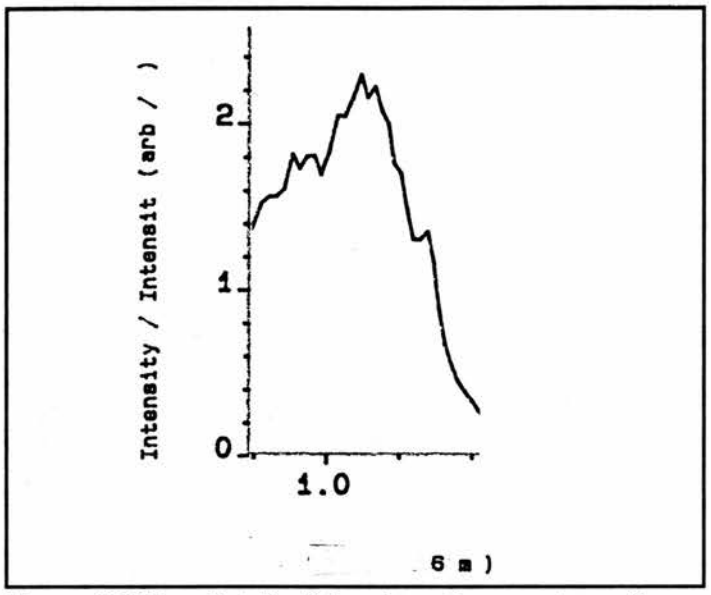

Figure 2.2[b] : Detail of the absorption spectrum of Cr^{4+}:*YAG*. showing the region of absorption between 950*nm* and 1100*nm*.

2.3 Fluorescence Spectrum of Cr^{4+}:YAG

The fluorescence spectrum of the crystal is given in figure 2.3. The crystal emits radiation between 1250*nm* and 1600*nm*. The spectrum is fairly flat between 1320*nm* and 1420*nm*. Self-absorption in the crystal results in a local reduction in the fluorescence intensity between 1450*nm* and 1500*nm*. This can be seen in figure 2.3. The residual signal at 1060*nm* is the result of the Nd:YAG laser which was used to pump the crystal when the fluorescence spectrum was measured.

Obviously, any laser can only be tuned in the region of fluorescence of the active medium. The broad fluorescence spectrum is one of the advantages of this source as it promises that Cr^{4+}:*YAG* will provide a laser tuneable within the region of 1250*nm* up to 1600*nm*.

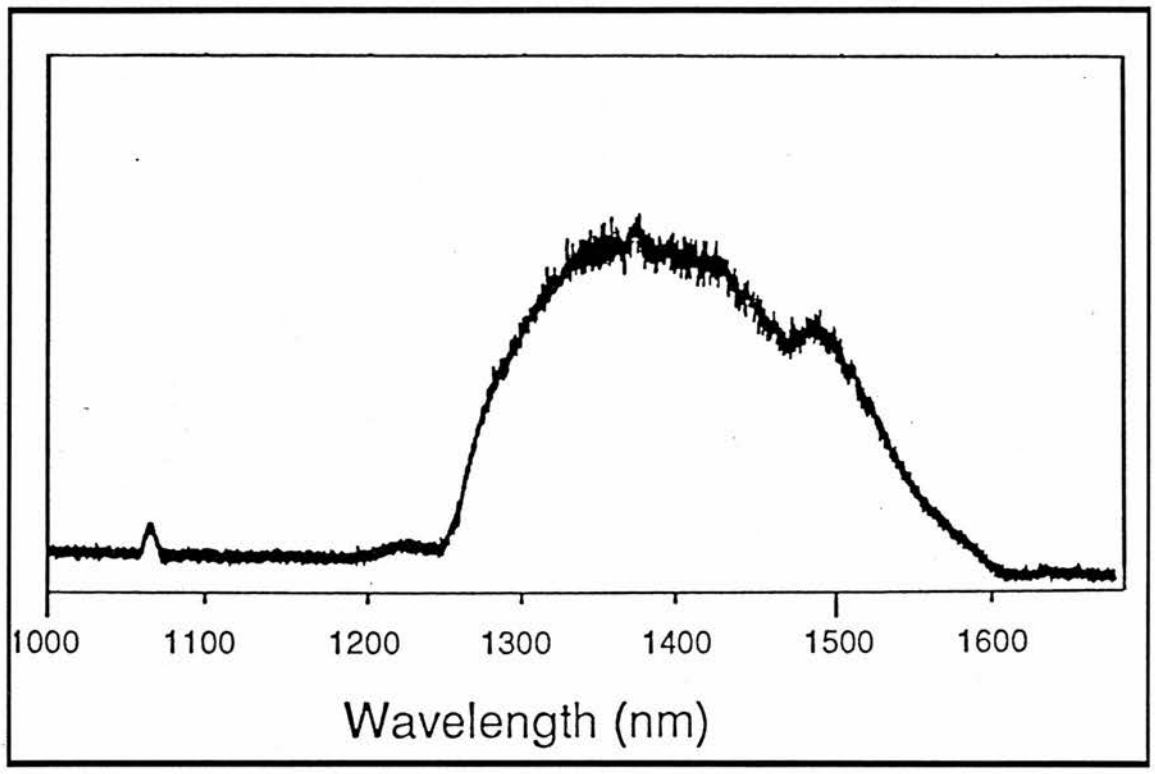

Figure 2.3 : Fluorescence spectrum of Cr^{4+}:*YAG*. The radiation at 1060*nm* was caused by the pump.

2.4 Polarisation of the Cr^{4+}:YAG-Crystal in the Brewster-angled cut Rod

In the experiments of Borodin and Shestakov a dependence of the energy characteristics of the Cr^{4+}:*YAG* laser on the mutual orientation of the crystal and polarisation of the exciting radiation was discovered. The maximal efficiency is obtained with the coincidence of the directions of the pumping wave polarisation vector from the fourth-order axes [100] or [010] upon excitation along the [001] axis. The Brewster-cut rod was therefore examined in the lasing system on its performance with the excitation of a polarised pump. The result is shown in figure 2.5. It can be seen that the minimum of the loss of the pump at the surfaces of the crystal coincides with the maximum lasing performance. This result, in addition to the observed efficiency near to the optimum values of 12% given by Borodin and Shestakov indicates that the crystal was cut in the

right way. The consideration about the orientation of the specific crystal used is therefore not necessary.

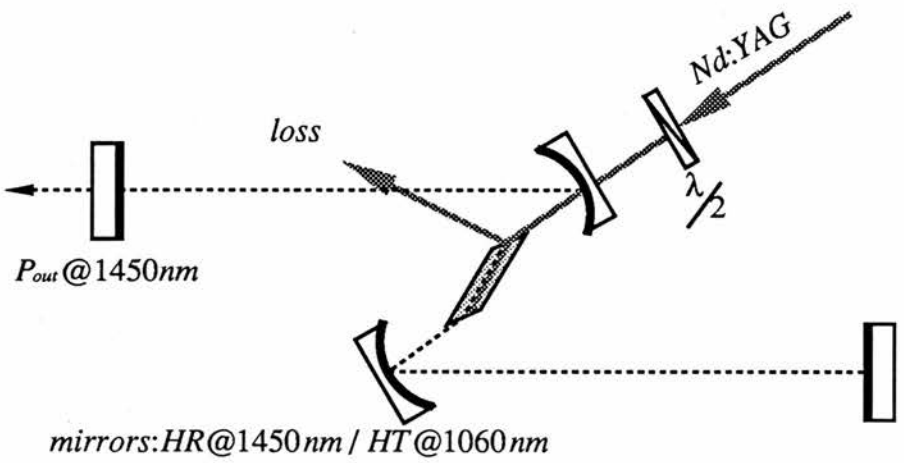

Figure 2.4 : The scheme employed to examine the dependence of the rod on the polarisation of the pump.

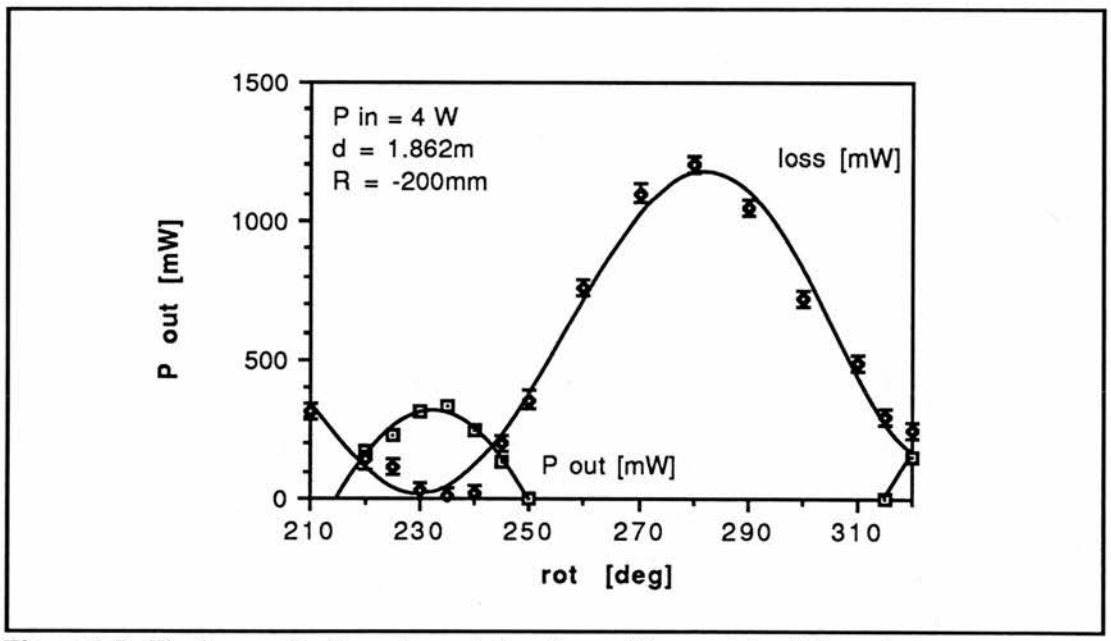

Figure 2.5 : The loss on the Brewster-angled surfaces of the crystal and the output power against the rotation angle of the λ/2-plate.

2.5 Conclusions

As a result of this experiments it is important to note that the fluorescence spectrum and the absorption spectrum have no overlap. This is desirable as an overlap of the absorption and the emission spectrum would only allow the use of a pump laser which is already lasing at the emitted wavelength and the emitted radiation of the active medium would be significantly decreased by self-absorption within the crystal without attributing to the output of the laser. The absorption band was found to be between 900*nm* and 1100*nm*. Therefore a Nd:YAG laser can be considered as a useful pump laser for this crystal.The emission band was found to be between 1250*nm* and 1600*nm*. This fairly broad range promises that Cr^{4+}:*YAG* is able to provide a source for a tuneable laser with emission in this range of wavelengths. Minor self-absorption effects can occur at wavelengths in the region of 1450*nm* but they are significantly smaller than the absorption of the crystal in the region of the pump laser. Moreover it is important to note that the orientation of the pump beam or of the crystal itself is important as far as efficiency is concerned. The specific crystal used was examined and experiments have shown that the crystal is orientated the right way in order to provide the optimum output.

2.6 References

1 Shestakov A.V. & al.: Tunable Cr^{4+}:*YAG* Lasers, *Conference on Lasers and Electro Optics*, CLEO Baltimore, Marryland, May 12-17 **1991**, Postdeadline-papers

2 Borodin & Shestakov, Izvestiya Akademii Nauk SSSR, Seriya Fizicheskaya, vol.54, No.8, p1500, **1990**

3. Cavity design

In the introduction the advantageous properties of all solid-state lasers operating in both CW and mode-locked configurations were discussed. In order to achieve optimum performance from such solid-state lasers, the cavity design parameters must be carefully chosen to match the properties of the given solid-state crystal. If they are not chosen correctly the laser may not give the maximum output power or may not oscillate at all. In this chapter the theoretical background of cavity design is discussed with regard to the astigmatic compensation of a cavity and the stability of the resonator in respects of its design parameters and the characteristics of a given pump laser.

3.1. Ray propagation

In order to calculate optimum cavity design parameters, it is first necessary to introduce a formal description of ray propagation. A paraxial optical ray propagating through various optical structures can be described by ray transfer matrices[1]. For this purpose it can be considered that a paraxial optical ray is determined by its distance to the optical axis r and its angle or slope r' with respect to that axis (see figure 3.1).

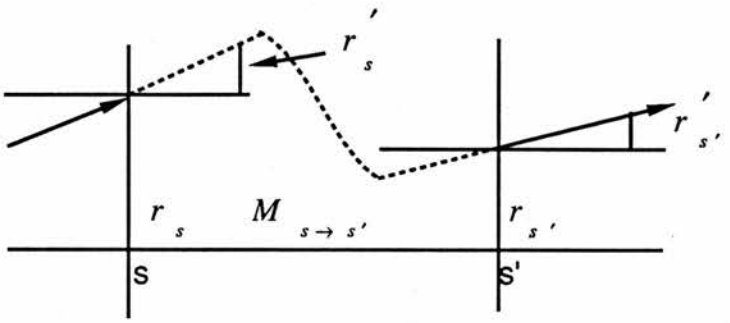

Figure 3.1: Parameters used to describe the propagation of a beam between two reference planes s, s'.

The propagation of a paraxial ray between two planes s and s' can then be described using the matrix transformation[2]:

$$\begin{pmatrix} r_{s'} \\ r'_{s'} \end{pmatrix} = M \begin{pmatrix} r_s \\ r'_s \end{pmatrix} \tag{3.1.1}$$

where $\begin{pmatrix} r_s \\ r'_s \end{pmatrix}$, $\begin{pmatrix} r_{s'} \\ r'_{s'} \end{pmatrix}$ refer to the beam parameters at reference planes s and s' respectively, and M refers to the transfer matrix.

3.2 Description of Optical Elements by Matrices

It is now possible to calculate the transfer matrix describing the propagation of a paraxial ray through several different optical elements. As the transfer matrix M only describes the propagation of a ray in a particular plane containing the z-axis, there exist different matrices for the same optical element dependent on the plane in which the ray propagation is being considered. In particular, the introduction of astigmatic elements into the cavity demands a different treatment for the sagittal (x-z-) and the tangential (y-z-) plane in the system (see figure 3.2) because the beam propagation is influenced to distinct degrees by astigmatic elements in these two different planes.

In order to be able to consider the problems associated with astigmatism in **section 3.4.3** two kinds of matrices are needed; one used to describe the propagation of the beam in the tangential plane and the other is used to describe the propagation of the beam in the sagittal plane.

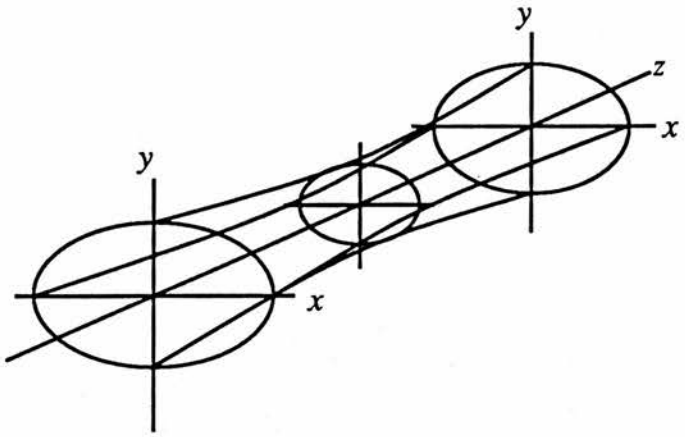

Figure 3.2: More complex beams need to be treated in different planes i.e. in the astigmatic case.

3.2.1 Matrices describing Special Optical Elements

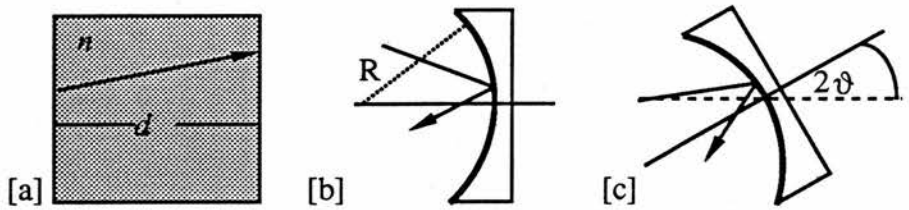

Figure 3.3: The different optical elements discussed in the text: [a]a propagation of a ray through medium with refractive index n, [b] mirror with radius of curvature R and [c] mirror inclined by an angle 2ϑ .

Non Astigmatic Elements

When a ray propagates through a non-astigmatic element, there is no difference in the propagation characteristics in either the sagittal or the tangential plane. The ray matrix M is therefore the same in both planes. The simplest such element corresponds to propagation through a medium with refractive index n as shown in figure(3.3.a).

The matrix in both planes is given by:

$$D_{d,n} = \begin{bmatrix} 1 & d/n \\ 0 & 1 \end{bmatrix} \qquad (3.2.1)$$

Reflection by a mirror with radius of curvature R as shown in figure (3.3.b) is also non-astigmatic, with the matrix in both planes given by:

$$R_R = \begin{bmatrix} 1 & 0 \\ -2/R & 1 \end{bmatrix} \qquad (3.2.2)$$

The reflection by a mirror with infinite radius of curvature is also the same in both planes (and it is the 2x2 identity matrix I_2).[3]

Astigmatic Elements

An element which introduces astigmatism is a mirror inclined by an angle 2ϑ as shown in Fig(3.3.c). Here it is necessary to discriminate between the sagittal and the tangential planes as follows:

$$I_{t,R,\vartheta} = \begin{bmatrix} 1 & 0 \\ -\dfrac{2}{R\cos\vartheta} & 1 \end{bmatrix}$$

and

$$I_{s,R,\vartheta} = \begin{bmatrix} 1 & 0 \\ -\dfrac{2\cos\vartheta}{R} & 1 \end{bmatrix} \qquad (3.2.3a,b)$$

where R is the radius of curvature of the mirror, 2ϑ is the angle of inclination and the indices t and s refer to the tangential and the sagittal plane respectively.

Another astigmatic element is the Brewster-angled laser rod.

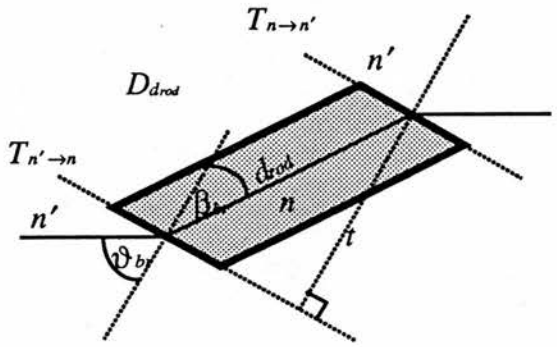

Figure 3.4 : The Brewster-angled rod and the notation used in the text: t is the thickness of the crystal, d_{rod} the geometrical length of the cut rod.

The ray transfer matrix $T_{n'\to n}$ describes the transformation of the beam propagating from medium of refractive index n' into a medium of refractive index n, at an inclined angle ϑ as shown in figure 3.4.

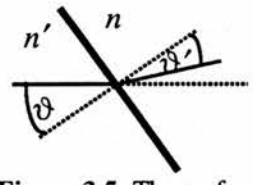

Figure 3.5: The surface inclined at ϑ of refractive index n.

This matrix is[4]

$$T_{n'\to n} = \begin{bmatrix} \dfrac{\cos\vartheta'}{\cos\vartheta} & 0 \\ 0 & \dfrac{n\cos\vartheta}{n'\cos\vartheta'} \end{bmatrix} \qquad (3.2.4')$$

In the sagittal direction it is (with $\vartheta = 0$)

$$T_{s,n'\to n} = \begin{bmatrix} 1 & 0 \\ 0 & \frac{n}{n'} \end{bmatrix} \qquad (3.2.4a')$$

and in the tangential plane (with $\vartheta = \vartheta_{brewster}$)

$$T_{t,n'\to n} = \begin{bmatrix} \frac{n'}{n} & 0 \\ 0 & \left(\frac{n}{n'}\right)^2 \end{bmatrix} \qquad (3.2.4b')$$

taking the approximation that $n' \equiv 1$ the matrices become

$$T_{t,n'\to n} = \begin{bmatrix} \frac{1}{n} & 0 \\ 0 & n^2 \end{bmatrix} \qquad T_{s,n'\to n} = \begin{bmatrix} 1 & 0 \\ 0 & n \end{bmatrix} \qquad (3.2.4a,b)$$

and

$$T_{t,n\to n'} = \begin{bmatrix} n & 0 \\ 0 & 1/n^2 \end{bmatrix} \qquad T_{s,n\to n'} = \begin{bmatrix} 1 & 0 \\ 0 & 1/n \end{bmatrix} \qquad (3.2.5a,b)$$

respectively.

Between these two entrance and exit transformations the beam has to pass a geometrical distance d_{rod} in the crystal. This must also be included in the overall crystal transformation matrix. If the physical crystal thickness is given by t, the geometrical distance d_{rod} is given by [5]

$$d_{rod} = t\sqrt{\frac{n^2+1}{n^2}}, \qquad (3.2.6)$$

then the total transformation matrix is[6]:

$$C_t = T_{n\to n'} \cdot D_{d_{rod}} \cdot T_{n'\to n} \qquad \text{with}$$

$$C_{t,t} = \begin{bmatrix} 1 & d_{rod}/n^3 \\ 0 & 1 \end{bmatrix} \qquad C_{s,t} = \begin{bmatrix} 1 & d_{rod}/n \\ 0 & 1 \end{bmatrix} \qquad (3.2.7a,b)$$

The matrices $C_{t,t}$, $C_{s,t}$ appear to have the same form as the matrix D_{d_t}, D_{d_s} with

$$d_t = \frac{d_{rod}}{n^3}$$
$$d_s = \frac{d_{rod}}{n} \qquad (3.2.8)$$

being the distances which the ray would have to propagate in an empty cavity in order to be comparable to the resonator with the crystal[7]. This is referred to as the effective length of the rod in the tangential and the sagittal plane respectively. Note that the geometrical distance d_{rod} is the same in both planes whereas the effective path lengths differ from each other. The effective path length is a virtual length and can also be derived from Snell's law by some simple geometrical considerations.

3.2.2 Combination of Different Elements by Ordered Multiplication of Matrices

The transformation of a ray passing through an optical element can be obtained by employing the appropriate matrix M_i for this element. In order to describe the transformation of a ray propagating through a system comprising various optical elements it is necessary to find a matrix describing the propagation of the ray through all these optical elements. This matrix $M_{1\to 2}$ which describes the transformation of a ray travelling through two optical elements e1, e2 with the matrices M_1, M_2 is found by multiplying these two matrices[8]

$$M_{1\to 2} = M_2 M_1 \qquad (3.2.9)$$

It follows by induction[9], that this general transformation matrix is always the ordered product of the matrices characterising the individual members of the chain. The matrix $M_{s\to s'}$ which describes the propagation of a ray from the reference plane s to the second reference plane s' through k optical elements, described by their individual matrices M_i is therefore

$$M_{s\to s'} \equiv M_R = \prod_{i=k}^{1} M_i \qquad :i \in [1,k]. \qquad (3.2.9')$$

3.2.3 Sequences

A system consisting of k optical elements which is going to be periodically applied to a ray is called a sequence. The ray experiences a transformation dependent only on the ray transfer matrix M_R . The ray transfer through n consecutive elements is therefore described by the n-th power of the matrix M_R of this arrangement[10].

Formally, the eigenvectors $\underline{e_k}$ and the eigenvalues λ_k (k=1, 2) of the matrix M_R are given by[11]:

$$\det(M_R - \lambda_k E_2) = 0$$

and

$$M_R \underline{e}_k = \lambda_k \underline{e}_k, \quad \lambda_k \neq 0 \qquad : k \in [1,2] \tag{3.2.10}$$

This leads to the following description of a ray. As the eigenvectors $\underline{e_k}$ (k=1, 2) form a basis for all rays, an arbitrary ray $\underline{r}$ can be expressed as a linear combination of the basis vectors:

$$\underline{r} = \sum c_k \underline{e}_k \qquad : c_k \text{ real} \qquad : k \in [1,2] \tag{3.2.11}$$

After n round trips in the cavity the ray has transformed into

$$\underline{r}_n = M_R^n \underline{r} = \sum_{k=1,2} \lambda_k^n c_k \underline{e}_k \tag{3.2.12}$$

A ray $\underline{r}$ will necessarily be confined within the system described by a certain M_R provided[12]

$$|\lambda_k| < 1 \quad . \tag{3.2.13}$$

Using the expression for the eigenvalues,

$$\lambda_{1,2} = \frac{A+D}{2} \pm \sqrt{\left(\frac{A+D}{2}\right)^2 - 1} \tag{3.2.14}$$

this then leads to the criterion that:

$$\frac{1}{2}\left|Trace(M_R)\right| < 1 \qquad (3.2.15)$$

for ray confinement.

3.2.4 Round-Trip-Matrix

When the beam propagates through an arrangement of mirrors and optical elements so that it comes back to the same point from where it enters the same sequence of optical elements each time, the propagation of the beam can be described by applying a Matrix M_R representing the whole sequence. This matrix describing the transformation of a whole sequence of optical elements is called the round-trip-matrix .

Figure 3.6: The round-trip-matrix represents all optical elements involved in a resonator.

This matrix allows more complex optical systems to be treated in a convenient way. For a symmetrical z-shape cavity according to figure (3.8) the round-trip-matrix M_R is:

$$M_R = \left(M_{\leftarrow} * M_{\rightarrow}\right)^2$$

with

$$M_{\rightarrow} = R * D_{d1} * I_{R,\vartheta} * D_{\frac{R-d_{rod}}{2}+\delta} * C_{1/2}$$
$$M_{\leftarrow} = C_{1/2} * D_{\frac{R-d_{rod}}{2}+\delta} * I_{R,\vartheta} * D_{d1} * R \qquad (3.2.16)$$

where the reference plane is chosen to be in the middle of the rod.

3.3. Gaussian Beam

3.3.1 Gaussian Beam

Unlike ideal plane waves, the intensity distributions of laser beams are not spatially uniform. Phase fronts are also slightly curved. The electrical field amplitude E of this coherent light satisfies the wave equation

$$\nabla^2 E + k^2 E = 0 \qquad : k = 2\pi / \lambda \qquad (3.3.1)$$

The equation for light travelling along the z-axis can be written as

$$E = \Psi(x, y, z) e^{-ikz} \qquad (3.3.2)$$

with Ψ being a slowly varying complex function which represents the transverse field distribution. Combining (3.3.1) and (3.3.2) leads to

$$\frac{\partial^2 \Psi}{\partial x^2} + \frac{\partial^2 \Psi}{\partial y^2} + \frac{\partial^2 \Psi}{\partial z^2} - 2ik\frac{\partial \Psi}{\partial z} = 0 \qquad (3.3.3.a)$$

or

$$\frac{\partial^2\Psi}{\partial x^2}+\frac{\partial^2\Psi}{\partial y^2}-2ik\frac{\partial\Psi}{\partial z}=0 \qquad (3.3.3.b)$$

provided that Ψ varies that slowly with z such that the second derivative of z can be neglected.

It can be shown that

$$\Psi = e^{-i\left(P+\frac{k}{2q}r^2\right)} \qquad (3.3.4)$$

represents a solution of (3.3.3.b) with $r^2 = x^2 + y^2$. Here $P(z)$ represents a complex phase shift and $q(z)$ is called the complex beam parameter which describes the Gaussian variation in beam intensity with the distance r from the optical axis, as well as the curvature of the phase front which is spherical near the axis. For convenience, two real parameters R and ω are introduced, which are related to the beam parameter q in the following form:

$$\frac{1}{q}=\frac{1}{R}-i\frac{\lambda}{\pi\omega^2 n} \qquad (3.3.5)$$

Inserting (3.3.5) into (3.3.4) shows the physical meaning of these parameters also shown in figure (3.7): $R(z)$ is the radius of curvature of the wave front intersecting the axis at z, $\omega(z)$ is the distance from the z -axis, at which the field amplitude $E(z)$ is down by a factor 1/e compared to its value on the axis. Therefore the parameter $\omega(z)$ is often referred to as "spot-size" of the beam. The parameter ω_0 is the minimum spot size or beamwaist. It is the beam spot size at the plane z =0.

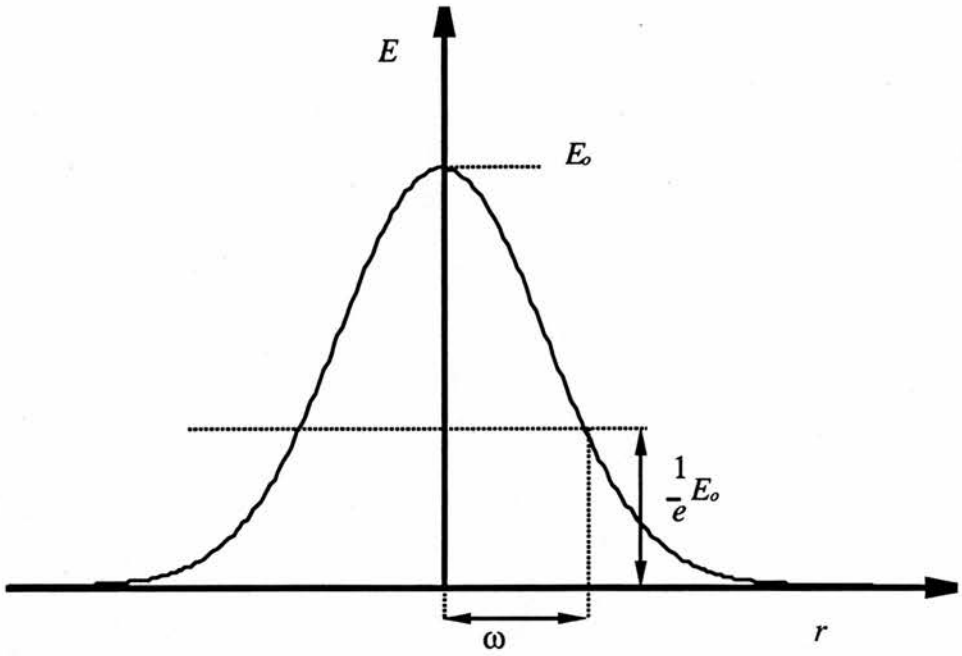

figure 3.7 : ω is the distance to the axis, where the field amplitude *E(z)* is down by a factor 1/e compared to its value on the axis.

3.3.2 ABCD-Law

It has been seen previously that the propagation of a ray through optical elements can be described by individual matrices M_i which transform the ray parameters. These same matrices also describe the propagation of Gaussian beams through these structures[13]. The parameter of the Gaussian beam is the complex beam parameter q which contains information about the spotsize ω and the radius of curvature R. This parameter is transformed by applying the following bilinear form

$$q_{s'} = \frac{Aq_s + B}{Cq_s + D} \tag{3.3.6}$$

where q_s, $q_{s'}$ are the complex beam parameter at the reference plane s, s' respectively and $\begin{pmatrix} A & B \\ C & D \end{pmatrix}$ represents the matrix of transformation between these two reference planes (compare figure 3.1). It follows by induction that the matrix describing more complex systems can also be applied to (3.3.6) and is found in the same manners as that described in **section 3.2.2**. This bilinear form (3.3.6) is referred to as an ABCD-law[14].

3.4 Resonator

An optical resonator consists of optical elements arranged in such a way that they can be used to build up large field intensities with moderate power inputs. An optical resonator can not be built with dimensions comparable to wavelength. Rays which bounce back and forth between the mirrors of a stable cavity experience a periodic focusing action[15]. A criterion of stability has therefore to be found. This section deals with the influences that different parameters have on the stability of a resonator, especially with regard to the symmetrical z-shape cavity.

3.4.1 Optical Resonator Algebra

In order to decide whether an optical resonator is stable or not, the self-consistency condition is applied. This is achieved by requiring that a stable eigenmode of the resonator is one that reproduces itself after each round-trip in the resonator. If q_s is the steady state complex beam parameter at a chosen reference plane s within the cavity, then applying the ABCD-law discussed in subsection 3.3.2 leads to:

$$q_s = \frac{Aq_s + B}{Cq_s + D} \qquad (3.4.1)$$

with $M_R=\begin{bmatrix} A & B \\ C & D \end{bmatrix}$ being the complete round trip-matrix starting and ending at the reference plane s. Solving for $\frac{1}{q_s}$ gives:

$$\frac{1}{q_s}=\frac{D-A}{2B}\pm\frac{\sqrt{(D-A)^2+4BC}}{2B}. \qquad (3.4.2)$$

As ω^2 in a Gaussian beam is always a finite positive number and with (3.3.5) it follows that the discriminant of (3.4.2) has to be considered negative.

As the round-trip matrix $M_R=\prod_i S_i \;:\; S_i \in SO_2$ and therefore of course $M_R \in SO_2$ it follows from the definition of the SO_2-group[16], that $\det(M_R)=1$. Therefore it follows from (3.4.1), (3.4.2) and comparing (3.3.5) to (3.4.2) that the criterion of stability of the resonator described by the round-trip-matrix M_R is

$$\frac{1}{2}|Trace(M_R)|<1 \qquad (3.4.3)$$

with the complex steady-state beam parameter being q_s from (3.4.1), (3.4.2). This is the same criterion as was found for rays which are not allowed to leave the sequence (see **section 3.2.3**). Comparing (3.4.3) to (3.4.2) gives

$$R=\frac{2B}{D-A} \qquad (3.4.4)$$

and

$$\omega^2 = \frac{\lambda}{\pi n} \frac{B}{\sqrt{1-(\frac{1}{2}Trace(M_R))^2}} \tag{3.4.5}$$

These are the radius of curvature R and the spot size ω at the reference plane chosen for (3.4.2)[17]. These parameters at different planes in the resonator can be found by applying the ABCD-law to q_S[18]. The stability of a resonator is therefore dependent on the various parameters connected with the trace of M where M is of course dependent upon the type of resonator that is employed.

3.4.2 Astigmatic Gaussian Beam

Gaussian Beams where

$$z_1 \equiv z_2 \Rightarrow \omega(x,z_1) \equiv \omega(y,z_2) \tag{3.4.7}$$

are referred to as circular Gaussian beams. The wave equation also permits solutions, where (3.4.7) is not satisfied and the beam spotsizes in the x- and the y-direction are different as indicated in figure 3.2:

$$E \propto e^{\left[-\frac{x^2}{\omega^2(x,z)}-\frac{y^2}{\omega^2(y,z)}\right]} \quad \text{with} \quad \omega(x,z) \neq \omega(y,z) \tag{3.4.8}$$

This is known as the elliptic Gaussian beam. This beam results from propagation through astigmatic optical elements. Thus, condition (3.4.7) defines the condition for astigmatic

compensation. (Astigmatism means that geometrical ray bundles in the sagittal plane behave differently than ray bundles in the tangential plane[19].)

3.4.3 Regions of stability

Regions of stability are given by parameter ranges within which the criterion of stability is satisfied. These are usually areas in the hyper planes in the vector space determined by the parameters of the cavity.

3.4.4 Astigmatic Compensation

As there are two different planes in the resonator a region of stability in each of them is found. It is important to note that stability in the sagittal plane does not necessarily imply stability in the tangential plane, so separate stability criterion for each plane must be found. Astigmatic effects generally occur in laser resonators where Brewster-angled surfaces are used together with off-axis mirrors. The combined effects of these elements in the cavity configuration used in this thesis will now be discussed.

Suitable Structure of the Cavity

In order to compensate for the astigmatic effect of the Brewster-angled crystal inside a cavity the cavity has to provide at least one other astigmatic element[20]. The idea is to design a resonator in which in the region of the crystal there is a maximal overlap of the tangential and the sagittal component of the beam[21].

In this thesis I will mainly discuss the properties of a 4-mirror symmetrical z-shape cavity with the parameters shown in figure (3.8). There are three different astigmatic elements involved in this arrangement so that astigmatic compensation is possible.

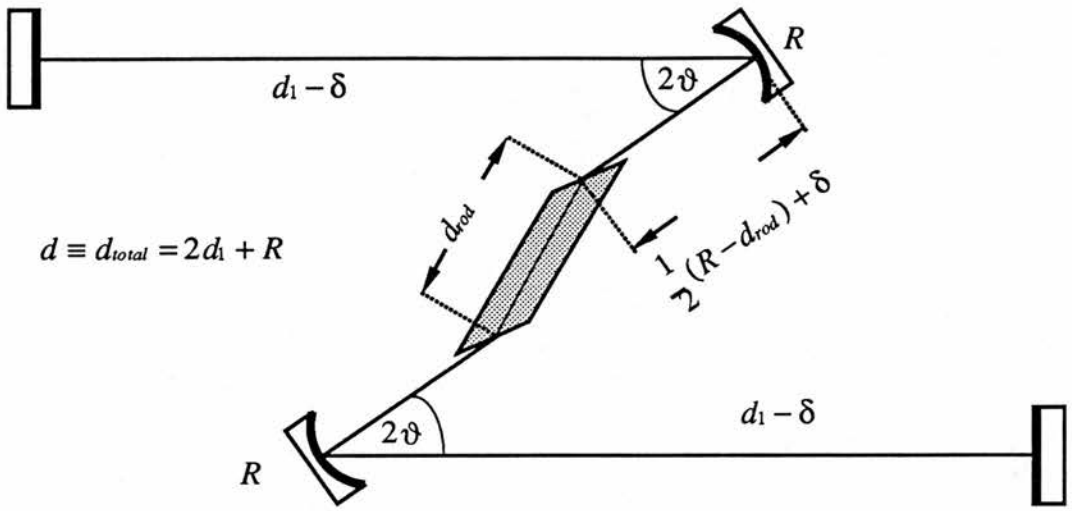

Figure 3.8 : The z-shape cavity and the in the text used parameters. The total length of the cavity is $d \equiv d_{total} = 2d_1 + R$.

3.4.5 Parameters

Applying the criterion of stability $\left|\frac{1}{2}Trace(M_R)\right| < 1$ shows that it is only the trace of M_R and therefore the parameters contained in $Trace(M_R)$ of the cavity which decide whether the cavity is stable or not. In the case of a symmetrical z-shape cavity these are:

$$Trace(M_R) = \Sigma(d, \vartheta, R, \delta) \qquad (3.4.10)$$

with the following cavity parameters determining stability:

[a] Angle of the Folding Section

The compensation of the astigmatism is easily achieved by setting a particular angle of compensation of the folding section ϑ^*. From [Kogelnik 1972][22] it can be seen that ϑ^* obeys the relation:

$$R \sin \vartheta^* \tan \vartheta^* = d_{rod} \frac{n^2 - 1}{n^3} \qquad (3.4.11)$$

for a z-shape cavity with R being the radius of curvature, d_{rod} being the geometrical length of the rod, ϑ^* being the required angle of compensation and n being the refractive index of the crystal (compare figure 3.8). Thus ϑ^* can be readily calculated and plotted as a function of n , d_{rod} or R.

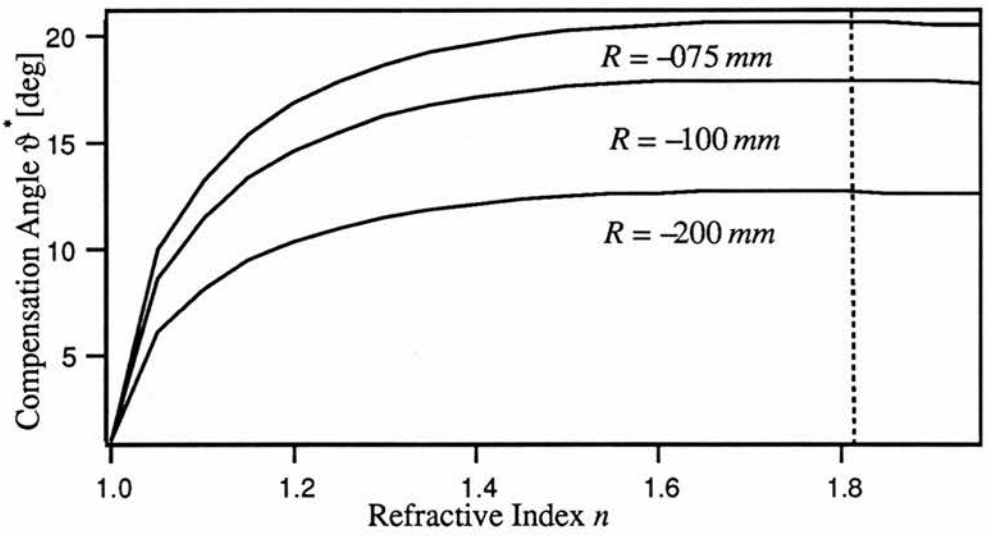

Figure 3.9 : Plot of ϑ^* as a function of refractive index n following (3.4.11) for R=-200*mm*, R=-100*mm* and R=-075*mm*. The line marks the value for n=1.82 (see also table 4.1) with d_{rod}=26*mm*.

[b] Position of the Mirrors of the Folding Section

Varying the position of the mirrors of the folding section by changing δ without changing the total length of the resonator d at all has also been used in the literature[23] to demonstrate regions of stability and the total overlap achieved by employing the right compensation angle. This is a very critical parameter and therefore plays quite a role as

far as alignment is concerned. The optimum δ^* is found by plotting the spotsize or the trace as a function of δ as shown in figure 3.10.

Stability in the tangential plane does not imply stability in the sagittal way as well and vice versa. An astigmatic compensated cavity is but one where the stability ranges in both planes are matched. In figure 3.10[a] an uncompensated cavity with an angle $\vartheta < \vartheta^*$ is shown. There is no overlap between the tangential and the sagittal plane. A totally compensated cavity with $\vartheta = \vartheta^*$ is shown in figure 3.10[b]. Here an optimum overlap between both planes is achieved. In figure 3.10[c] a cavity with $\vartheta > \vartheta^*$ is shown in which an overlap exists, but it is not maximised and by reducing the angle a more stable position could be achieved. The numerical treatment of this aspect is studied in section 4.3.1.1.

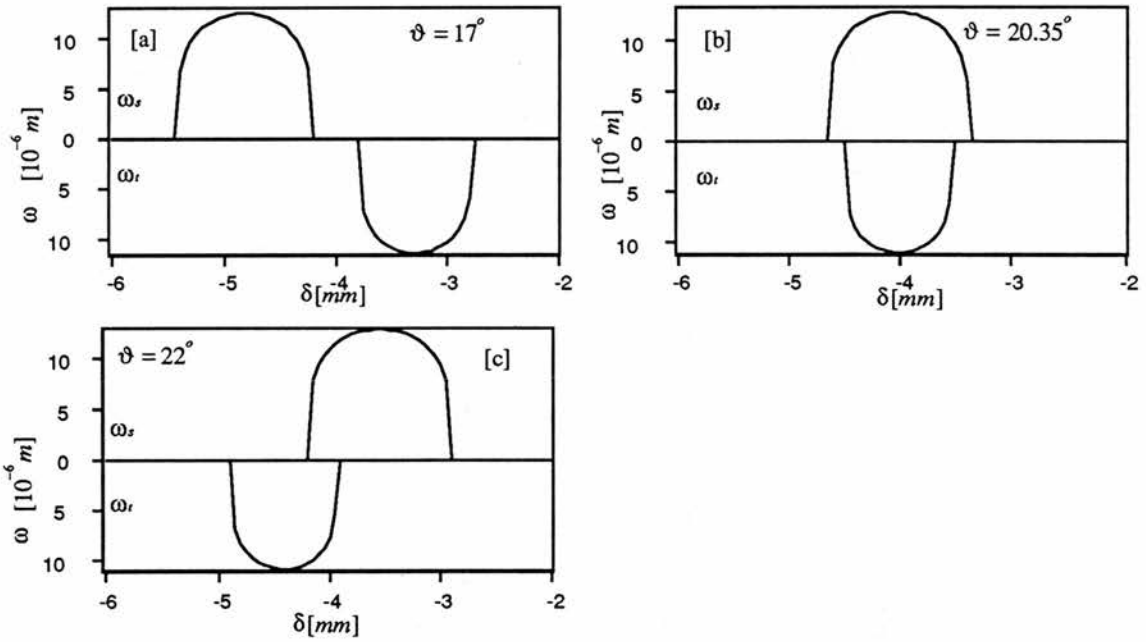

Figure 3.10 : Typical plots of the spotsize ω in the tangential and the sagittal plane as a function of δ . The parameters used were R=-075*mm*, d_{rod}=26*mm*, *d*=1.40*m* in a z-shape four mirror cavity: [a] shows a non compensated cavity at ϑ=17° with no overlap of the stability ranges in the sagittal and the tangential plane, [b] at ϑ=20.35° shows the fully compensated cavity with the maximum overlap and [c] at ϑ=22° shows a non-optimally compensated cavity with some overlap. [cp. Kogelnik 1972][24].

[c] Total Length of the Cavity

Unlike δ and ϑ the total length d of the resonator is a non-astigmatic parameter of stability. The stability range of a given cavity will decrease for longer cavity lengths d. Therefore, for longer cavities, the more difficult alignment becomes. As d changes, δ will also change so that the focus becomes tighter for longer cavities. Also, it is important to note that divergence effects towards the edges of the rod become significant. Therefore the volume of the signal in the rod undergoes a change and plotting the volume versus d shows that there is in general also an optimum length of the cavity. (For treatment in more detail see section 4.3.1.1.2).

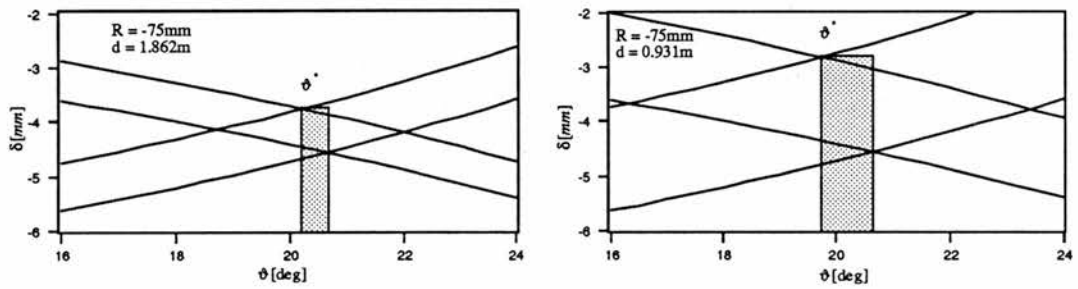

Figure 3.11 : Plot of δ versus ϑ. The stability range for the longer cavity becomes significantly smaller.

As a result of all these effects there exists an optimum radius of curvature R^* for a given length of the cavity.

[d] Radius of Curvature

The main effect of the radius of curvature R is the focusing of the signal in the crystal. The smaller the absolute radius of curvature is, the more tightly focused the beam waist in the middle of the crystal becomes and the more divergent the beam is towards the edges (figure (3.12)). The volume inside the crystal is a measure of the efficiency of the laser

output[25] for cw operation. This has to be considered and minimised. Therefore the variation of R is very useful as the total length d is determined by suitability for mode locking.

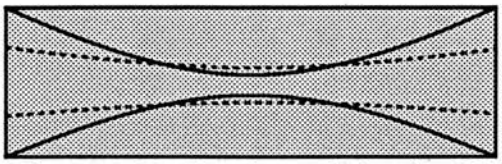

Figure 3.12: The shape of the signal beam within the crystal and the beamwaist influence the volume taken up in the crystal.

Because of the multiplication of the matrices in order to obtain the round-trip matrix, it is not very useful to consider the trace of the round-trip matrix analytically. The stability criterion will be discussed in more detail in connection with the computing of the specific values for the given sets of parameters in **section 4.2.1.**

3.4.6 Radiation Volume inside the Crystal taken up by the Signal

The most important cavity design parameter besides the compensation angle ϑ^* for cw-operation is the volume which the signal beam occupies within the rod. It is possible to calculate the volume of the signal beam within the crystal after having been provided with all the cavity design parameters in the following way:

$$V_{rod} = \int_0^{d_{rod}} \int_0^{2\pi} \Omega(\varphi, z) d\varphi dz \qquad (3.4.12)$$

with $\int_0^{2\pi} \Omega(\varphi, z) d\varphi$ being the cross-sectional area normal to z described by the spot sizes ω_φ in the φ-direction. A satisfactory approximation will be the area of the ellipse $\pi\omega_s\omega_t$ so that the volume can be written as:

$$V_{rod} \approx \pi \int_0^{d_{rod}} \omega_s(z)\omega_t(z) dz \qquad (3.4.13)$$

For this volume a minimum has to be found so the performance of the laser is the most efficient in this configuration[26]. Altering this volume can be achieved by changing the cavity parameters as discussed above. Whereas the compensation angle ϑ^* and the relative adjustment of the folding section δ will be determined by the length of the cavity d, the length d itself appears to be the parameter which can be used to find a minimum volume.

A common application of the z-shape cavity is to obtain pulses by mode locking the system. The length of a mode locked laser cavity is usually constrained by properties of the acousto-optic devices. Therefore the total length of the cavity d is better treated as a fixed quantity and the optimum R is the calculated.

3.5 Pump beam

The beam of the pump laser also occupies a specific volume inside the crystal. This area is embedded in the area taken up by the signal as the wavelength of the pump is smaller than the wavelength of the signal. This volume has also to be considered and minimised.

3.5.1 Influence of the Pump Laser on the Efficiency of the System

The efficiency of the pump beam is mainly determined by its ability to match a given signal beam within the cavity, or to be more precise, within the crystal. As in the case of the volume of the signal within the crystal, it is the volume of the pump beam within the crystal which has also to be minimised[27]. This can be done by varying the parameters of the pump beam, which will be discussed in this section.

3.5.2 Volume inside the Crystal taken up by the Pump beam

The parameters of the pump which are determining the volume of the pump within the rod (see figure (3.13)) are:

$$V_{pump} = V_{pump}(\Delta, f, R, q_{pump}) \qquad (3.5.1)$$

with Δ being the distance between the surface of the crystal and the lens, f being the focal length of the crystal, R being the radius of curvature of the mirror between lens and crystal and q_{pump} being the complex beam parameter of the pump at the plane of the lens.

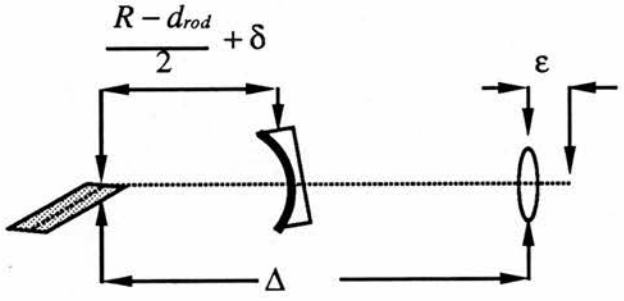

figure 3.13 : The parameters connected with the pump Δ, f, R. ε is the difference between the theoretical distance f and Δ $f = \Delta + \frac{d_{rod}}{2} + \varepsilon$

Because q_{pump} and R are fixed, f and Δ have to be chosen in order to minimise the volume of the pump. Applying the ABCD-law gives for q in a plane s' within the crystal that:

$$\omega_{s'}^2 = \frac{\lambda}{\pi n} \frac{1}{\mathrm{Im}\left(q_{s'}^{-1}\right)} \qquad (3.5.2)$$

Scanning through the rod and computing ω_t, ω_s provides all the necessary values to calculate the volume V_{pump}. In the symmetrical case, the minimum of a fixed set-up is always the one at which the beam waist of the pump is in the middle of the rod due to the divergence at the ends of the rod as shown in figure 3.14. The minimum volume for several specific given sets is therefore found by comparing the beam waist and the spotsize at the edges of the crystal for each set. If the beam waist of the pump is in the middle of the rod, the parameters of the minimum volume have been found.

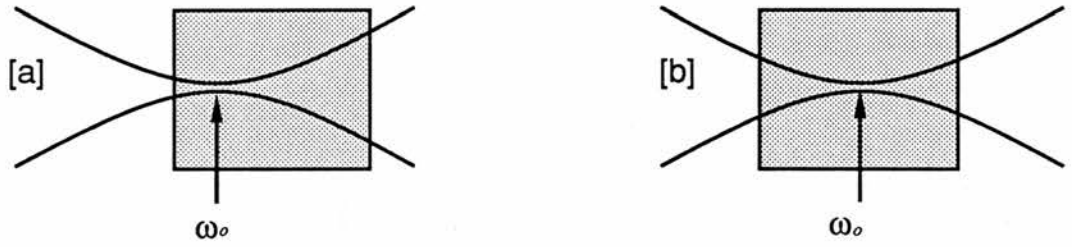

Figure 3.14 : The effect of the divergence towards the edges of the rod can be used to find the optimum parameters of the pump: the volume is minimised when the beamwaist is found in the middle of the rod. The volume in [a] is higher than the volume in [b].

3.6 Conclusions

In this chapter the essential theoretical background for cavity design was given. In order to provide a stable cavity the criterion of stability (equation 3.4.3) was found and the parameters which determine the trace of the round-trip matrix were introduced. The

volume taken up by the signal- and the pump-beam inside the active laser medium was considered to be an important parameter. It is best to be minimised. In the next chapter the criterion of stability will be applied to the concrete optical elements and the experimental results will be presented.

3.7 References

1 Kogelnik, H.: *The Bell System Technical Journal*, p.455, March **1965**

2 Kogelnik,H. & Li, T.: *Applied Optics*, vol.5, No.10, p.1550, **1966**

3 For all these matrices see: Yariv, A.: Optical Electronics, Third Edition, Japan **1985**; Siegman, A.E.: Lasers, Mill Valley, California **1986;** Kogelnik, H.: *Applied Optics*, vol.4, No.12, p.1562, **1965**; Hanna, D.C.: *IEEE J. of Quantum Electronics*, vol. QE-5, No.10, p.483, **1969**

4 Hanna, D.C.: *IEEE J. of Quantum Electronics*, vol. QE-5, No.10, p.483, **1969**

5 Kogelnik, H. & al.: *IEEE J.of Qantum Electronics*, vol. QE-8, No.3, p.373, **1972**

6 Hanna, D.C.: *IEEE J. of Quantum Electronics*, vol. QE-5, No.10, p.483, **1969**; Kogelnik, H.: *Applied Optics*, vol.4, No.12, p.1562, **1965**

7 Kogelnik, H. & al.: *IEEE J.of Qantum Electronics*, vol. QE-8, No.3, p.373, **1972**

8 Siegman, A.E.: Lasers, Mill Valley, California **1986;** Yariv, A.: Optical Electronics, Third Edition, Japan **1985** ; Kogelnik, H.: *Applied Optics*, vol.4, No.12, p.1562, **1965**

9 Yariv, A.: Optical Electronics, Third Edition, Japan **1985**

10 Kogelnik,H. & Li, T.: *Applied Optics*, vol.5, No.10, p.1550, **1966**; Siegman, A.E.: Lasers, Mill Valley, California **1986**; Yariv, A.: Optical Electronics, Third Edition, Japan **1985**

11 Koecher, M.:Lineare Algebra und analytische Geometrie, Berlin, Heidelberg, New York, Tokyo **1985;** Kowalsky, H.-J.: Lineare Algebra Berlin, **1984**; Lorenz, Falko Lineare Algebra II, Mannheim, Wien, Zürich (**1989**); Nef, W.: Lehrbuch der Linearen Algebra, Basel, **1977**

12 Kneubühl, F.K. & Sigrist, M.W.: Laser Stuttgart **1991**

13 Kogelnik,H. & Li, T.: *Applied Optics*, vol.5, No.10, p.1550, **1966**

14 Yariv, A.: Optical Electronics, Third Edition, Japan **1985**; Siegman, A.E.: Lasers, Mill Valley, California **1986**

15 Kogelnik,H. & Li, T.: *Applied Optics*, vol.5, No.10, p.1550, **1966**

16 Koecher, M.:Lineare Algebra und analytische Geometrie, Berlin, Heidelberg, New York, Tokyo **1985;** Kowalsky, H.-J.: Lineare Algebra Berlin, **198;**; Lorenz, Falko Lineare Algebra II, Mannheim, Wien, Zürich (**1989**); Nef, W.: Lehrbuch der Linearen Algebra, Basel, **1977**

17 Kogelnik, H.: *Applied Optics*, vol.4, No.12, p.1562, **1965**

18 Yariv, A.: Optical Electronics, Third Edition, Japan **1985**; Siegman, A.E.: Lasers, Mill Valley, California **1986**

19 Kogelnik,H. & Li, T.: *Applied Optics*, vol.5, No.10, p.1550, **1966**

20 Dunn, M.H. & Ferguson, A.I.: *Optics Communication*, vol.20, No.2, p.214, **1977**; Kogelnik, H. & al.: *IEEE J.of Qantum Electronics*, vol. QE-8, No.3, p.373, **1972**

21 Kogelnik, H. & al.: *IEEE J.of Qantum Electronics*, vol. QE-8, No.3, p.373, **1972**; for concrete treatment see **section 4.2.1**

22 Kogelnik, H. & al.: *IEEE J.of Qantum Electronics*, vol. QE-8, No.3, p.373, **1972**; Hanna, D.C.: *IEEE J. of Quantum Electronics*, vol. QE-5, No.10, p.483, **1969**; Dunn, M.H. & Ferguson, A.I.: *Optics Communication*, vol.20, No.2, p.214, **1977**

23 Kogelnik, H. & al.: *IEEE J.of Qantum Electronics*, vol. QE-8, No.3, p.373, **1972**

24 Kogelnik, H. & al.: *IEEE J.of Qantum Electronics*, vol. QE-8, No.3, p.373, **1972**

25 Digonnet, M.J.F. & Gaeta, C.J.: Applied Optics, Vol24, No.3, p.333, 1985

26 Digonnet, M.J.F. & Gaeta, C.J.: Applied Optics, Vol24, No.3, p.333, 1985

---

27 Digonnet, M.J.F. & Gaeta, C.J.: Applied Optics, Vol24, No.3, p.333, 1985

4. Experimental Characteristics of CW Laser Operation

The stability criteria discussed in chapter 3 can now be employed to calculate a set of parameters corresponding to the most efficient astigmatic compensated cavity design. These theoretical results are compared with the experimental values obtained. This chapter also includes a description of the experimental equipment and its limitations.

4.1. Cavity Elements

4.1.1 Mounting of the Crystal

A 26*mm* long Brewster-angled cut Cr^{4+}:*YAG* Czochralski-grown crystal prepared with Cr^{4+}-concentration of about $5 \cdot 10^{17} cm^3$ was used as the active medium in the laser[1]. The refractive index is n=1.82 (see figure 4.1).

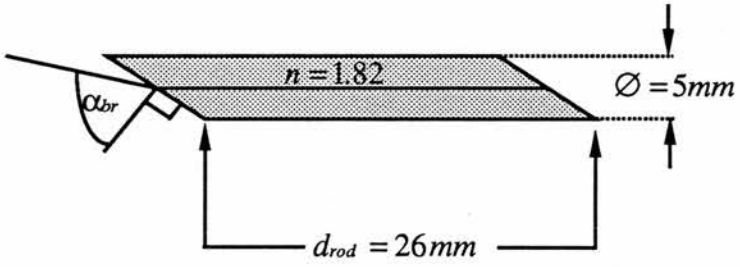

Figure 4.1: The key geometrical values of the Cr^{4+}:*YAG* -crystal.

The crystal was fixed in a copper housing with translational and rotational adjustment to permit easy intracavity alignment. The housing was connected to two pipes which provided cooling water. The water was cooled down by a simple beer-cooler which was only able to control the temperature to $\pm 3^{\circ}C$ but it was found that this was not too critical. Poor thermal contact between the crystal surfaces due to the roughness of the

copper is avoided by using a thin sheet of soft indium metal between the crystal and the copper holder. The water cooled the housing but was not in direct contact with the crystal or the indium. The housing was designed so it was only the polished faces of the crystal which were able to be seen from outside (figure 4.2).

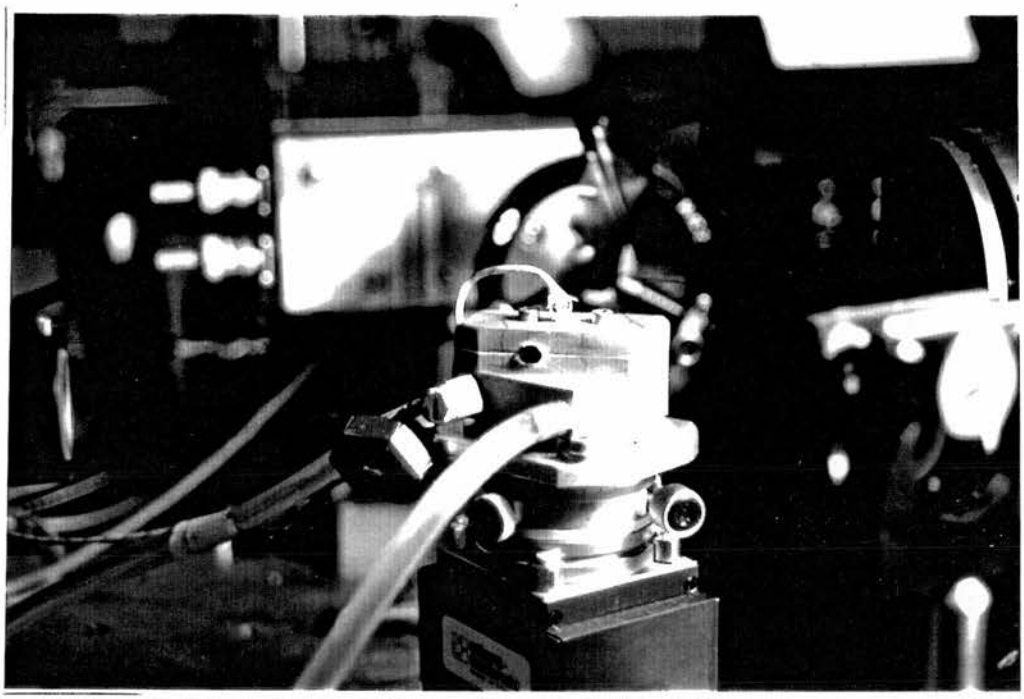

Figure 4.2 : A photograph showing the mounted crystal.

On the top of the housing a tiny hole of about a diameter of 1mm was drilled to give access to the crystal where a finger of a thermometer was situated in order to monitor the temperature of the crystal. The crystal was oriented so that the Brewster-angled faces were in the tangential- or the *y*-*z*-plane (see figure 3.8).

It was found after 6 months that the crystal lost material at the edges of the exposed end closest to the pump due to the fact that cooling was less efficient in this area and accidentally misaligned pump-beams would melt these areas off. This problem was solved by pushing the crystal a few mm back into the housing at the side of the pump-

beam entering and provided a shield and therefore better cooling for the end surface from then on.

4.1.2 Pump Laser

In order to excite the atoms in the Cr^{4+}:*YAG* rod a pump laser must be chosen which emits power in the wavelength of the absorption of the crystal (figure 2.2) between 900*nm* and 1100*nm*. Therefore a Nd:YAG laser[2] operating @1064*nm* was used.

The Nd:YAG laser uses trivalent neodymium ions (Nd^{3+}) which are present as the dopant in yttrium aluminium garnet (YAG $=Y_3Al_5O_{12}$). The laser emission occurs at $\lambda_o = 1.0641\mu m$ at room temperature.

The laser used was a *Control* laser with an average power in cw operation of 6*W*. In cw operation the Nd:YAG laser rod is arc-lamp pumped[3]. A typical arrangement uses a highly polished elliptic cylinder in order to concentrate the light from the lamp, which is placed along one focal axis, onto the laser rod, which occupies the other axis. The reflecting mirrors are placed outside the cylinder.

4.1.3 Mirror sets

Because of the relatively unknown properties of the Cr^{4+}:*YAG* crystal a large degree of flexibility was desired in the design and construction of the laser resonator. Therefore different mirrors of various radii of curvature R for the folding section R=-75mm, R=-100mm and R=-200mm were used. Because the system was pumped with a Nd:YAG laser @1064nm these mirrors were chosen to be highly transparent (HT) @1064nm and highly reflective (HR) @1450nm. The transmission curves (figure 4.21) which came with the mirrors show that reflection of 99.8% was achieved for wavelengths between 1450*nm*

and 1500*nm*. Between 1350*nm* and 1560*nm* there was still a residual reflection of 99%. The transmission @1064*nm* was 98.5%. The end mirrors were chosen to be a plane mirror with HR@1450nm and output-couplers of T=1%, 3%, 4% and 5% were used.

4.2. Cavity Stability Considerations

In order to get the most efficient cw-operation of the laser, the parameters of the cavity have to be chosen such that it produces the smallest volume V of the signal inside the crystal[4]. It is also necessary to consider the astigmatic compensation to guarantee a stable cavity[5]. In this thesis a symmetrical z-shape cavity has been considered (see figure 3.8). Therefore the compensation angle ϑ^* for the different mirror set-ups was computed. Also the area of the beam at the beam waist in the middle of the rod was found by determining the sagittal and the tangential component of the beam and the volume of the signal within the crystal of these parameters was calculated.

4.2.1 Numerical Computation

In order to decide whether a cavity is stable, the criteria of stability (equation 3.4.3) has to be checked numerically. Therefore the position of the mirrors of the folding section is varied by changing the relative adjustment of the mirrors in the folding section δ (compare figure 3.8) whereas all other parameters are fixed. The beamwaist ω is only well defined within a certain range of stability $S_{s,t} = [\delta_{\min}, \delta_{\max}]_{s,t}$ in the tangential and in the sagittal plane such that the following equivalence holds:

$$\delta \in S_{t,s} \Leftrightarrow \left| trace(M_{R_{t,s}}) \right| < 2. \qquad (4.3.1)$$

In this case the stability range[6] can easily be seen by plotting ω_s, ω_t as a function of δ as shown in figure 4.3 (compare also figure 3.10).

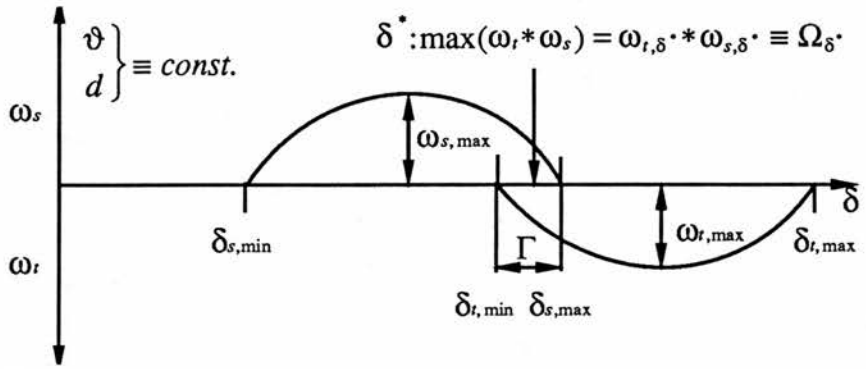

Figure 4.3 :Typical plot of ω_s, ω_t as a function of the relative adjustment of the mirrors in the folding section δ. Note the different parameters involved in the calculation $\delta_{i,j}$, Γ, δ^* and Ω. The angle ϑ and the total length of the cavity d are fixed.

The laser is stable in both planes only in the area of overlap Γ which describes an interval $[\delta_1, \delta_2]$ with $\delta_1 < \delta_2$. The sign of Γ is defined by

$$\Gamma = \max(\delta_{t,\max}, \delta_{s,\max}) - \min(\delta_{t,\min}, \delta_{s,\min}) - |S_t| - |S_s| \quad (4.3.2)$$

with

$$|S|_{s,t} = [\delta_{\max} - \delta_{\min}]_{s,t} \quad (4.3.3)$$

and therefore stability is only achieved if Γ is negative:

$$\textit{Stability} \Rightarrow \Gamma < 0 \quad (4.3.4)$$

The cross-sectional area $\pi\Omega$ is defined by

$$\Omega(\delta) = \omega_{t,\delta} \cdot \omega_{s,\delta} \quad (4.3.5)$$

This area $\pi\Omega$ is only defined as long as $\Gamma<0$. Choosing the maximum $\pi\Omega$ out of a given set by only varying δ leads to $\Omega_{\delta\cdot}$ (see figure 4.3) with

$$\Omega_{\delta\cdot} = \omega_{t,\delta\cdot}\,\omega_{s,\delta\cdot} = \max(\Omega_\delta) \;: \qquad \delta \in [S_t, S_s] \qquad (4.3.6)$$

This parameter $\Omega_{\delta\cdot}$ is a measure of the maximum of the intensity of the beam in the middle of the rod. The variation of the beam area in the middle of the rod $\Omega_{\delta\cdot}$ as a function of the off-axis angle of the mirrors of the folding section ϑ and the total length of the cavity d is shown in figure 4.4 in a 3-dimensional plot as $\Omega_{\delta\cdot} = \Omega_{\delta\cdot}(\vartheta, d)$ for all the three different sets of mirrors available. Ω also gives the range of stability dependent on ϑ and d as wherever $\Gamma < 0 \Rightarrow \Omega \neq 0$. The detailed discussion of these plots is given in section 4.2.1. At this stage it is enough to notice the decrease of $\Omega_{\delta\cdot}$ with increasing cavity lengths d and the decrease of the range of the angle ϑ in which the cavity fulfils the criteria of stability of equation 3.4.3 with shorter focal length mirrors.

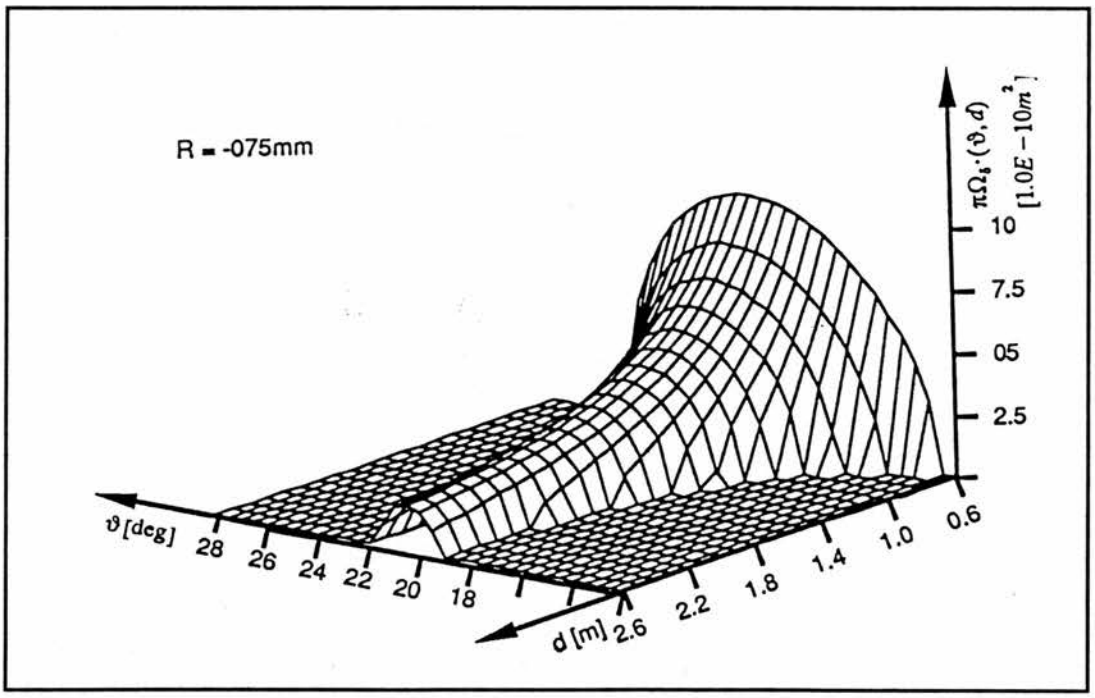

Figure 4.4a: Plot of $\pi\Omega$ as a function of ϑ and d for R=-075*mm*.

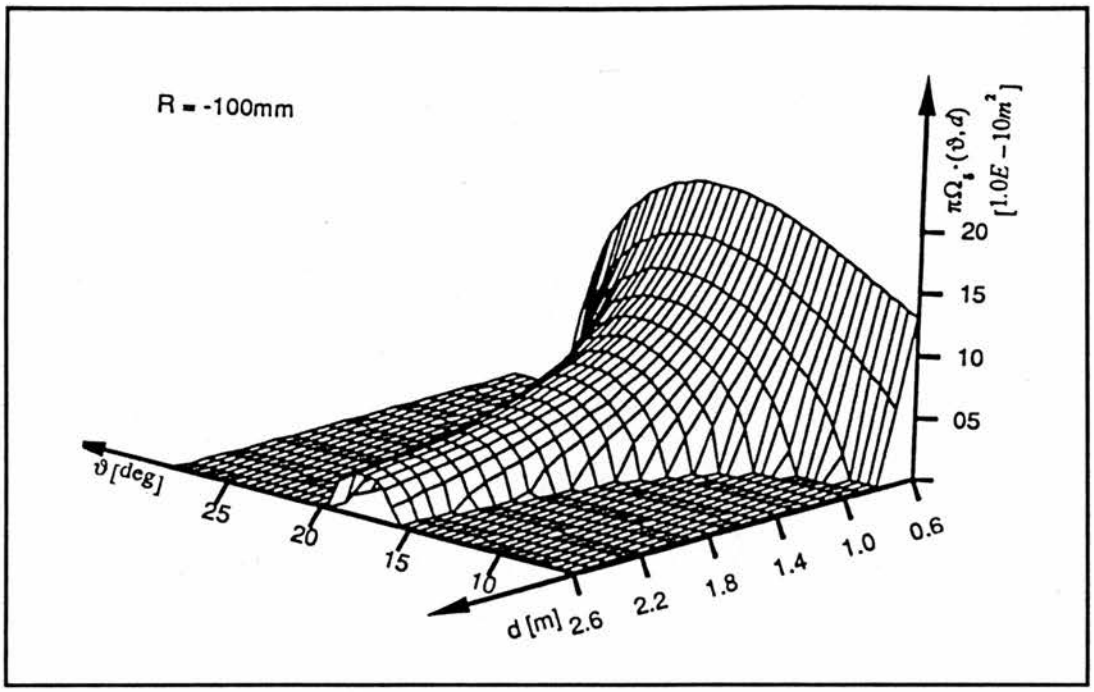

Figure 4.4b: Plot of $\pi\Omega$ as a function of ϑ and d for R=-100*mm* .

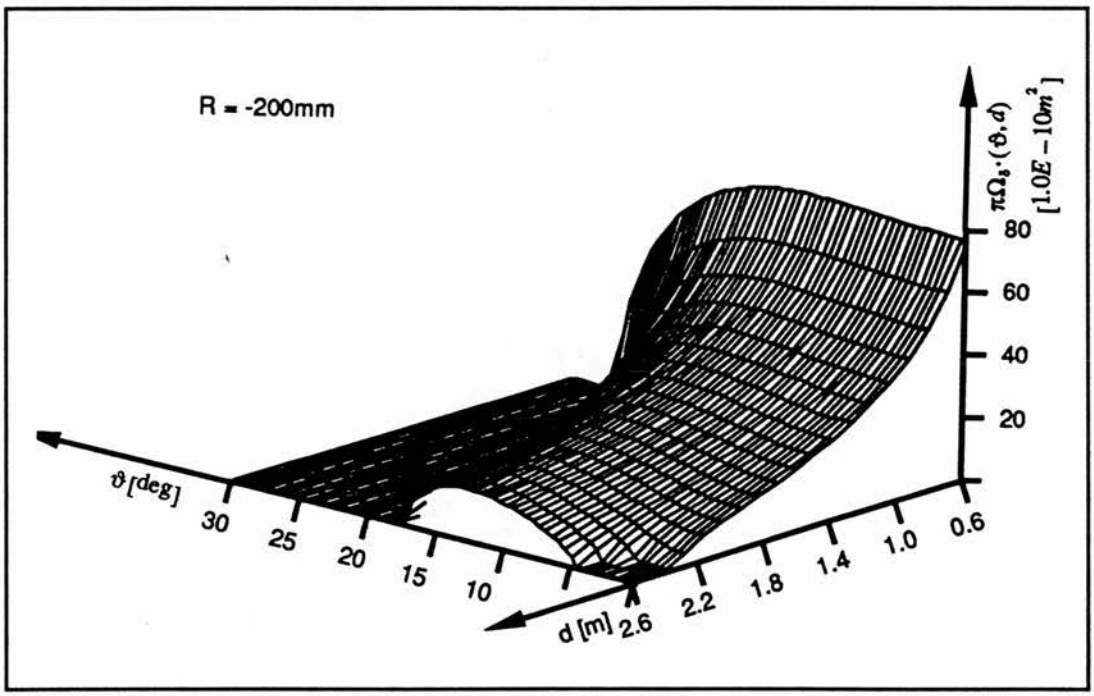

Figure 4.4c: Plot of $\pi\Omega$ as a function of ϑ and d for R=-200*mm* .

As the cross-sectioned area Ω varies within the crystal the volume of the signal within the crystal V^* described by

$$V^*(\vartheta,d,\delta^*)=\int_{z_1=-\frac{1}{2}d_{rod}}^{z_2=\frac{1}{2}d_{rod}}\pi\Omega(\vartheta,d,\delta^*,z)dz \qquad (4.3.7)$$

will not behave in the same way as Ω does. The plot of $V^*(\vartheta,d,\delta^*)$ is shown in figure 4.5 for all the three different sets of mirrors R=-075*mm*, R=-100*mm*, R=-200*mm*. In all plots a maximum volume $\overline{V}$ =2.5E-10m^3 has been chosen and only the volume smaller than $\overline{V}$ is plotted. The particular behaviour of this parameter is also to be discussed in section 4.2.1. At this stage it is worth considering that the regions where the volume V is less then $\overline{V}$ is found in larger areas of d and ϑ the higher the absolute value of the radius of curvature R becomes. It is also important to note that there is a minimum volume for each set of mirrors for a certain length of the cavity and that the angle ϑ becomes more critical for longer cavities.

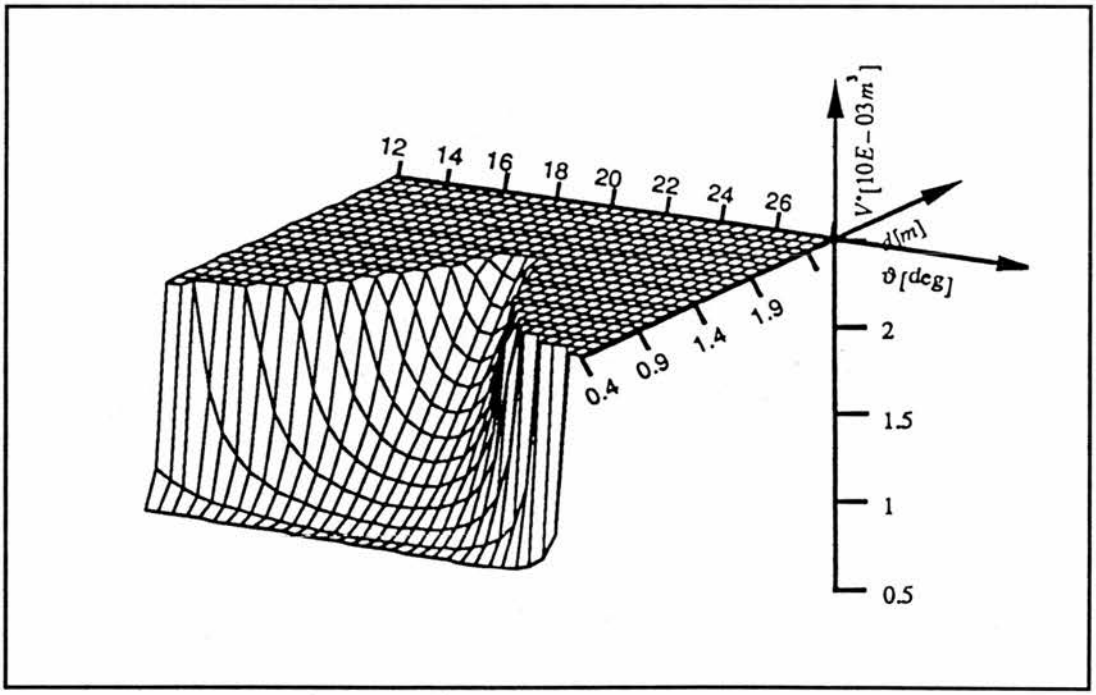

Figure 4.5a: Plot of V as a function of ϑ and d for R=-075*mm* .

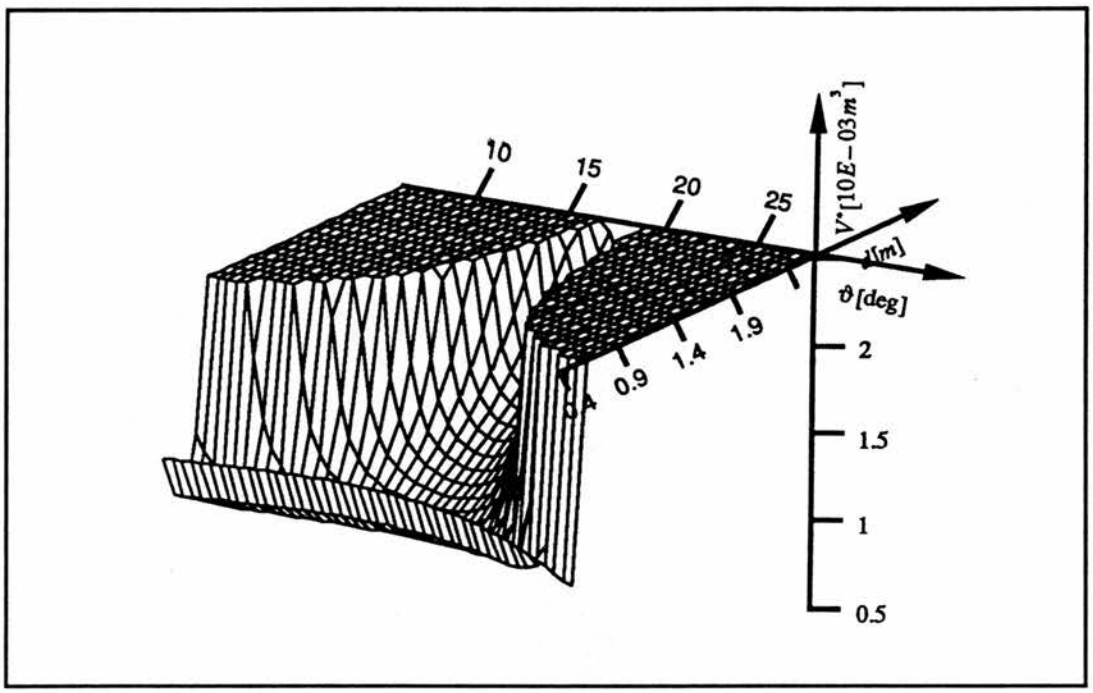

Figure 4.5b: Plot of V as a function of ϑ and d for R=-100*mm* .

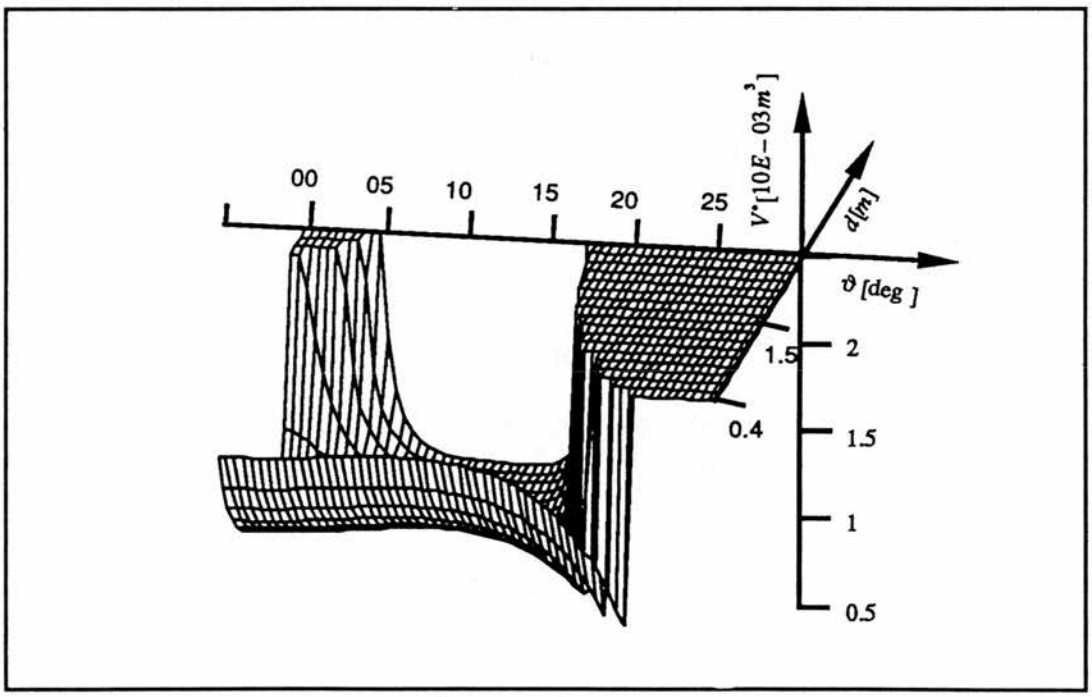

Figure 4.5c: Plot of V as a function of ϑ and d for R=-200*mm* .

In the next section the behaviour and the dependence of mainly these two parameters on R, d, and ϑ will be examined.

4.2.1.1 Dependence on ϑ

The angle ϑ (compare figure 3.8) is an important variable as far as astigmatic compensation is concerned. The optimum angle for astigmatic compensation $\vartheta^* = \vartheta^*(n, R, d_{rod})$ is the angle for which the highest overlap Γ between the sagittal and the tangential plane takes place for a given set of parameters . Whereas in the treatment of the compensation angle in [Dunn-Ferguson 1977] and [Kogelnik 1972] the approximation of the equality of sagittal and tangential stability ranges S defined in equation 4.3.3 ($S_s \approx S_t$ and therefore ϑ^* was well defined) is used, the parameters of a z-shaped cavity with d_{rod}=26mm does not allow this approximation (see figure 3.10[b]). Here the respective stability ranges are not equal ($S_s \neq S_t$) as S is a function of the effective propagation length of the beam[7]. This explains the different influence on the stability ranges S in both the sagittal and the tangential plane. There exist 3 different definitions of ϑ^* as $\Gamma(\vartheta^*) = \Gamma_{\max} \equiv -\min[S_t, S_s]\big|_{d,R}$ for $\vartheta^* \in [\vartheta_1, \vartheta_2]$:

$$
\begin{aligned}
&[a] \quad \vartheta_a^*: \delta_{s,\min}(\vartheta^*) \equiv \delta_{t,\min}(\vartheta^*) \\
&[b] \quad \vartheta_b^*: \omega_{s,\max}(\vartheta^*) \equiv \omega_{t,\max}(\vartheta^*) \\
&[c] \quad \vartheta_c^*: \delta_{s,\max}(\vartheta^*) \equiv \delta_{t,\max}(\vartheta^*)
\end{aligned}
\qquad (4.3.8)
$$

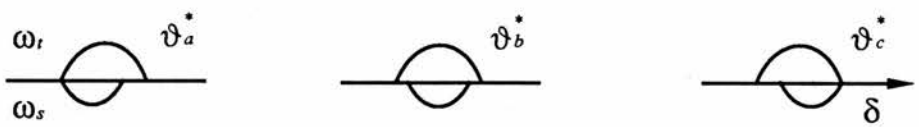

Figure 4.6 : The stability plots for the three different definitions according to figure 4.3.

The first definition 4.3.8[a] is equivalent to that of [Kogelnik 1972] and [Dunn-Ferguson 1977] as the difference of $S_{t,s}$ is not considered. ϑ^* is in this case as shown in equation

3.4.11 independent of the total length of the cavity d. The values for ϑ^* obtained from equation 3.4.11 with n=1.82 and d_{rod}=26mm are listed in table 4.1.

d [m]	1.862			0.931		
R [mm]	-075	-100	-200	-075	-100	-200
ϑ_a^* [deg]	20.66	17.75	12.74	20.66	17.75	12.74
ϑ_b^* [deg]	20.42	17.48	12.28	20.18	17.15	11.65
ϑ_c^* [deg]	20.20	17.22	11.92	19.74	16.64	10.83
$\Delta\vartheta^*$[deg]	0.46	0.53	0.82	0.92	1.11	1.91

Table 4.1 :The optimum angle of astigmatic-compensation according to (4.3.8.a,b,c) calculated with n=1.82 and drod=26mm . For the longer cavity the difference between the different definitions in (4.3.8) becomes smaller.

This definition represents the solution of one special ϑ^* and it is the maximum of all ϑ^*'s. Only provided $S_s \approx S_t$ this ϑ^* is the only angle of compensation. In the case of $S_s \neq S_t$ all possible angles of compensation with $\Gamma(\vartheta^*) \equiv \Gamma_{max}$ are within an interval $[\vartheta_c^*, \vartheta_a^*]$. It is therefore also useful to find the specific values for ϑ_c^* in order to describe the dependence of the chosen system in terms of the range the compensation angle ϑ^* can vary in.

Even if Γ doesn't change within $[\vartheta_c^*, \vartheta_a^*]$ there are other parameters of stability which do. This is for example the cross-sectional area of $\pi\omega_s\omega_t$, which in neither of the cases 4.3.8[a] or 4.3.8[c] has reached its maximum. This maximum of the cross-sectional areas is defined by 4.3.8[b], because this definition matches the possible maximum of the beamwaist ω_o of the tangential and the sagittal plane. This is also the angle of compensation which is well between the two values 4.3.8[a] and 4.3.8[c] which represent the edge of the solution. This definition 4.3.8[b] is therefore used in this thesis to find the

compensation angle $\vartheta^* \equiv \vartheta_b^*$. This ϑ^* is other then 4.3.8[a] dependent on the total length of the cavity *d*.

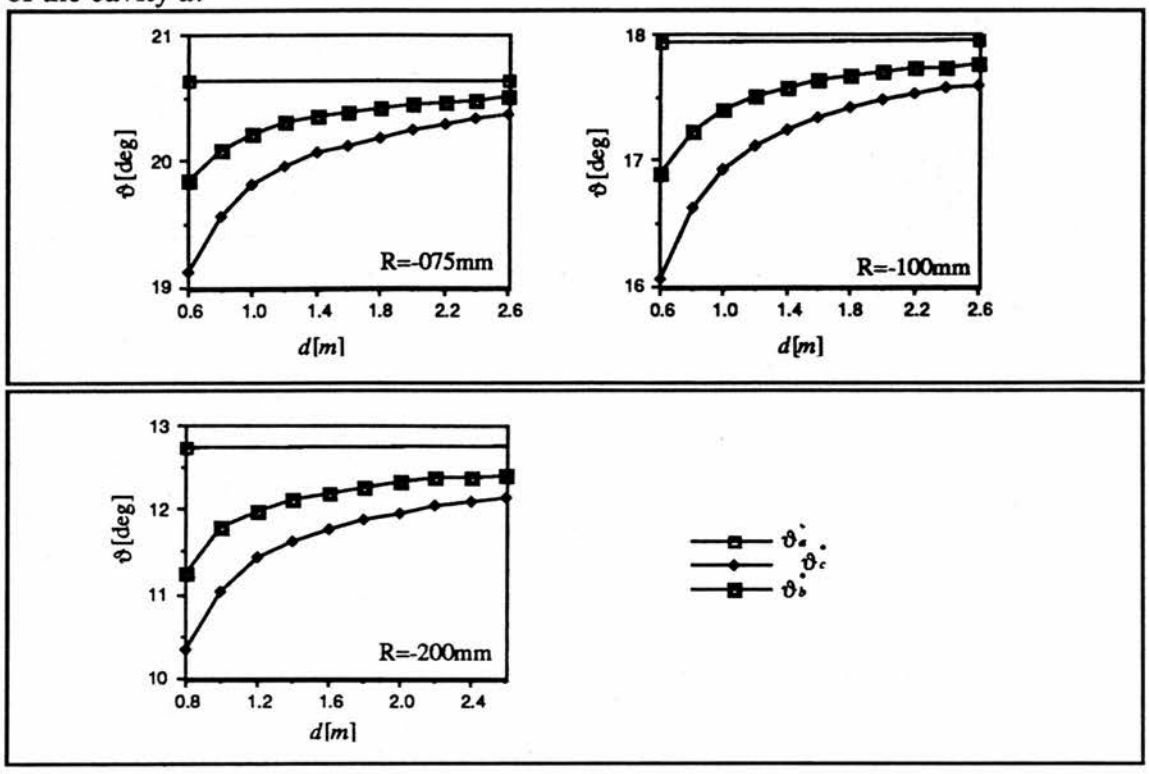

Figure 4.7: Plot of ϑ^* as a function of *d* for all R's. The different possible angles of compensation result in an interval of angles in which the cavity is compensated.

At the optimum astigmatism compensation angle ϑ^* the corresponding beam waists ω_{t,δ^*} in the tangential and ω_{s,δ^*} in the sagittal plane are at δ^* at its maximum. The product of ω_s, ω_t - Ω - is therefore also at its maximum at ϑ^*. This can be seen in figure 4.8.

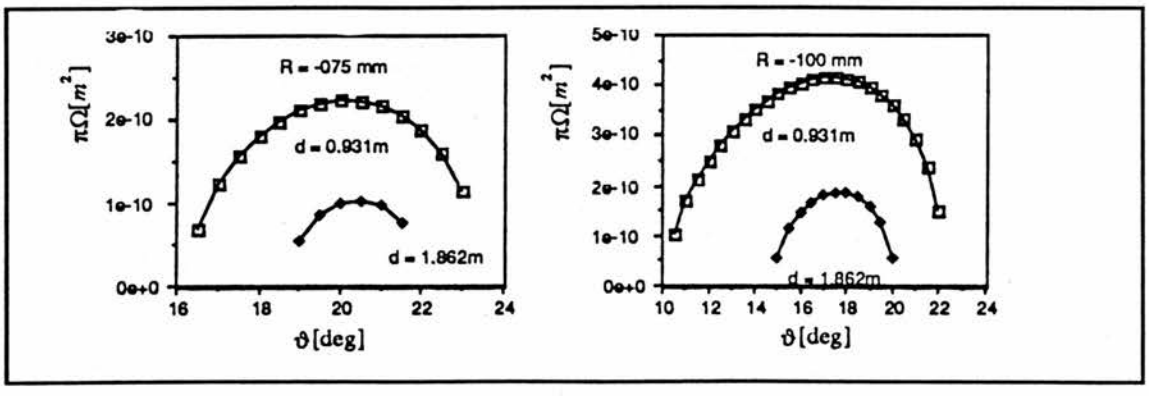

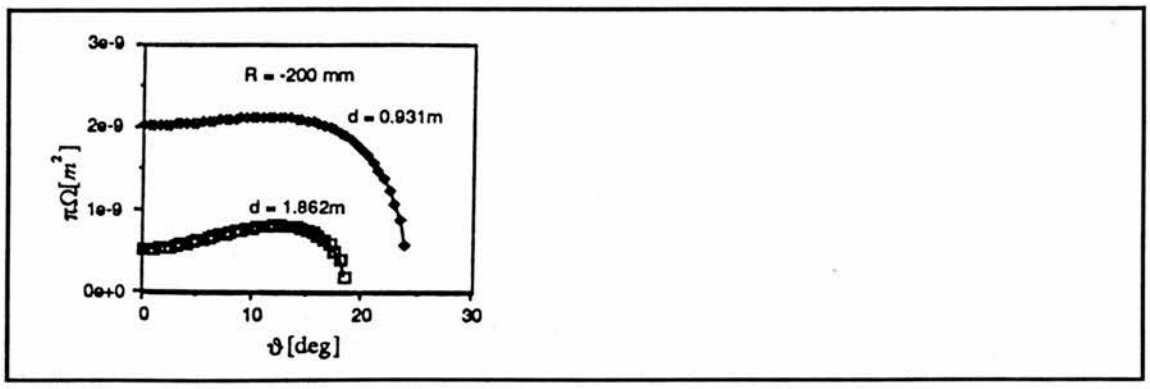

Figure 4.8: Plot of $\pi\Omega$ as a function of ϑ for all given R's.

The volume occupied by the signal inside the crystal V^* is also dependent on the astigmatic effect. The closer ϑ is to ϑ^* the smaller the volume becomes. This is due to the fact that the presence of astigmatism the symmetric inside the crystal is disturbed and therefore the divergence of the beam towards the edges adds a lot more to the volume than in the symmetrical case. Only in the case of the R=-200*mm* the beam is less tightly focused so that divergence effects don't increase the volume where it is not totally astigmatically compensated (compare figure 4.9 and figure 3.12)

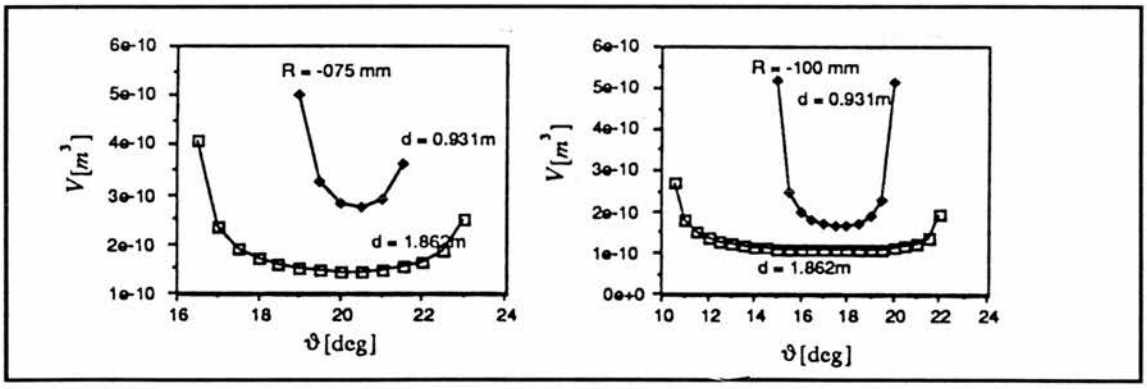

Figure 4.9[a] : Plot of V^* as a function of ϑ for R=-75*mm* and R=-100*mm*.

ϑ^* and the compensation of the cavity is therefore determined by the radius of curvature R, the shape of the cavity (here: z-shape), the correct position of the mirrors of the folding section expressed by δ^* and the total length of the cavity d (see figure 3.8).

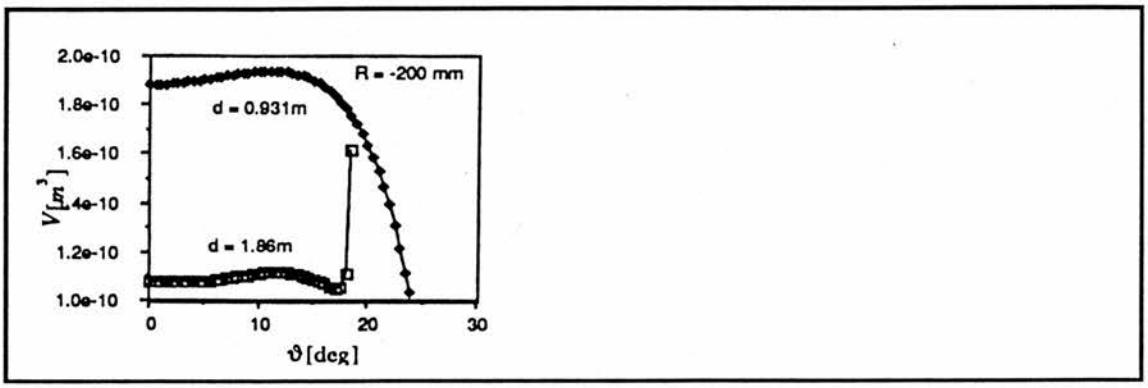

Figure 4.9: Plot of V^* as a function of ϑ for R=-200*mm* and for all given R's.

4.2.1.2 Dependence on *d*

The weakest influence of all parameters on the compensation of the astigmatic effect is the total length of the cavity d. While it does not so much influence the optimum compensation angle ϑ^* it does influence the other parameters Γ, δ^*, Ω and the volume V^*.

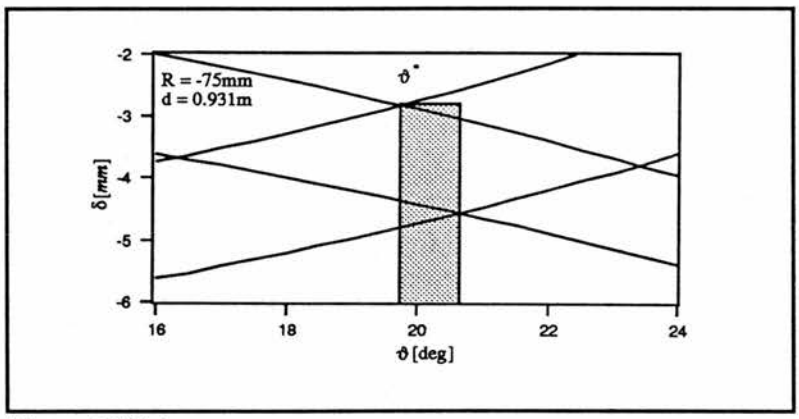

Figure 4.10[a]

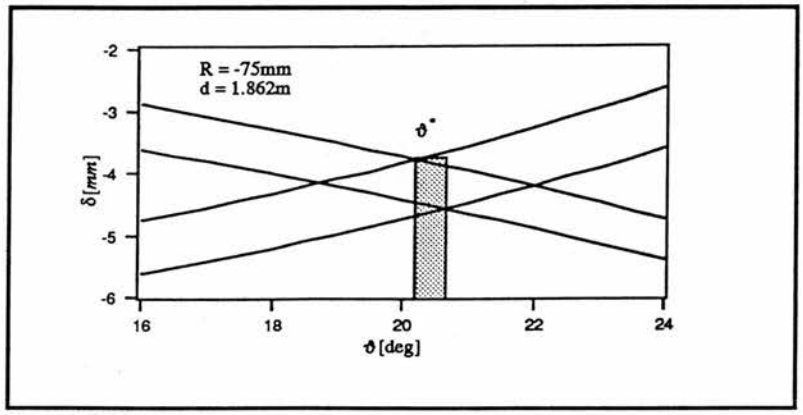

Figure 4.10[b]

Figure 4. 10 : Stability area of δ versus ϑ with fixed length of the cavity d=1.862m and d=0.931m and fixed radius of curvature R=-075mm. Note the significant reduction of the region of stability for the longer cavity.

The stability range S and therefore the overlap Γ become smaller the longer the cavity is chosen as can be seen in figure 4.10 and figure 4.11. This means that alignment of the laser becomes more difficult for longer lengths of the cavity.

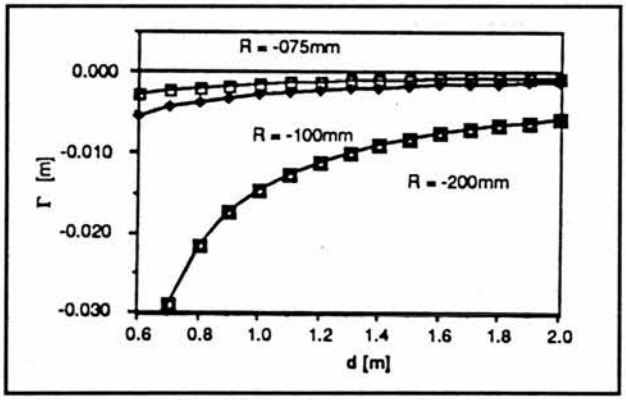

Figure 4.11 : Plot of the overlap Γ as a function of the total length of the cavity d for all given sets of mirrors R=-075mm, R=-100mm and R=-200mm.

On the other hand the position of mirrors becomes closer as the cavity is extended (figure 4.12). This leads to a tighter focus inside the crystal for longer cavities and therefore Ω decreases with d (figure 4.13).

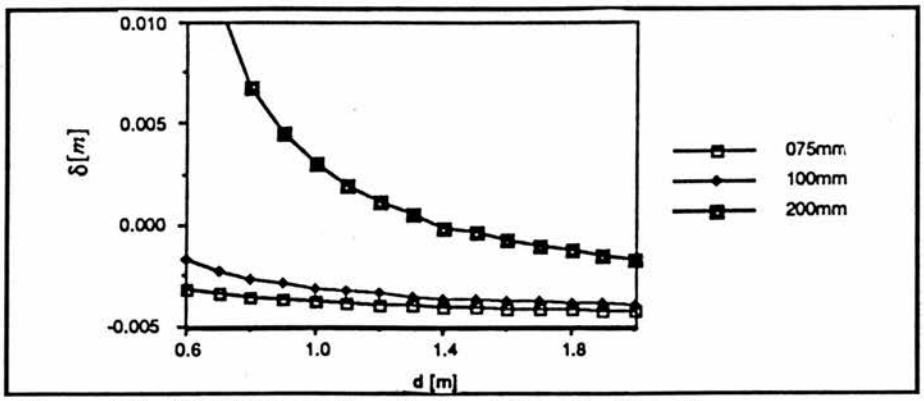

Figure 4.12 : Plot of the relative adjustment δ as a function of the total length of the cavity *d* for all given sets of mirrors R=-075*mm*, R=-100*mm* and R=-200*mm*.

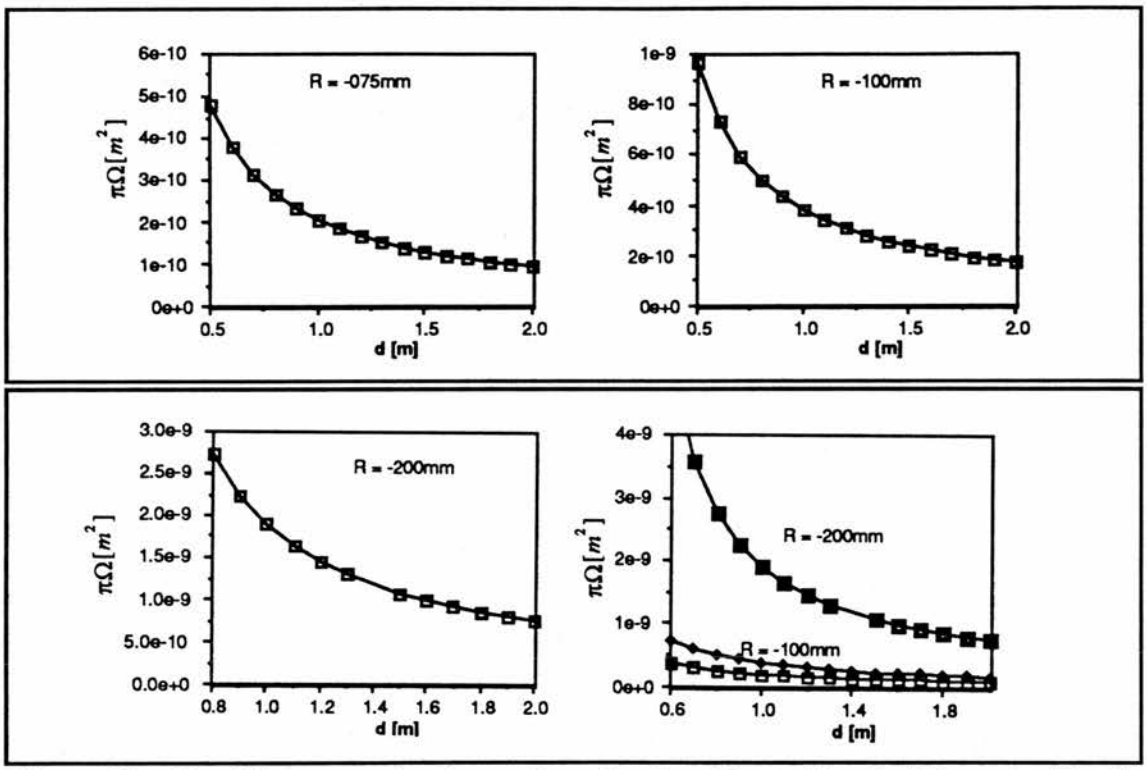

Figure 4.13 : Plot of the cross-sectional area πΩ as a function of the total length of the cavity *d* for all given sets of mirrors R=-075*mm*, R=-100*mm* and R=-200*mm*.

In order to predict the behaviour of the volume as a function of *d* note that with a tighter focus, the area in the middle of the crystal Ω_{δ^*} is made smaller but on the other hand the divergence towards the edges of the crystal is increased by the decrease of δ^*. This effect is shown in figure 4.14 and in figure 3.12. The tighter the focus becomes the larger the

effect of divergence becomes. Both of these effects have to be considered when minimising the volume V.

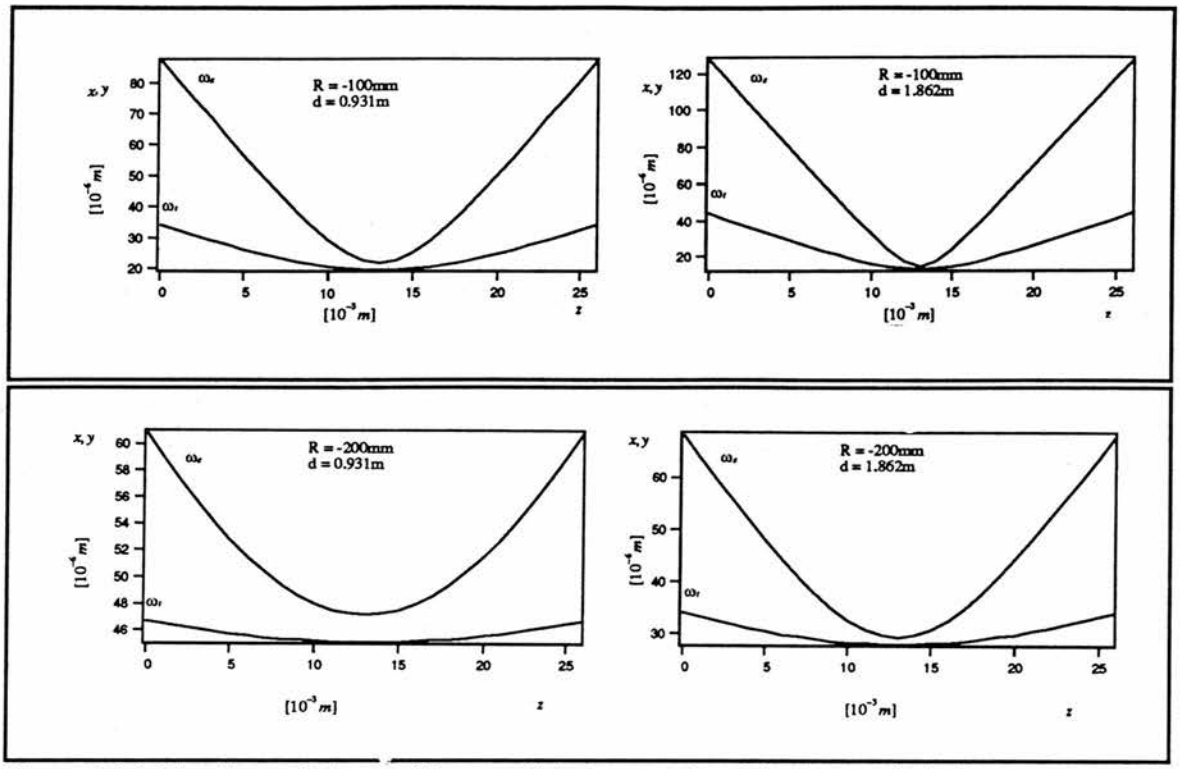

Figure 4.14: The shape of the signal beam within the crystal and the beamwaist influence the volume taken up in the crystal. These theoretical plots show the spot sizes of the signal beam inside the rod in the tangential and the sagittal plane. Notice that in the case of R=-200*mm* [b] the effect of divergence for longer cavities is not as significant as in the case of R=-100*mm*.[a]

The plots of the volume V^* are shown in figure 4.15 for all available sets of mirrors. Each set of mirrors has its own length of compensated z-shape cavity in which a minimum of the volume of the signal inside the rod is found. The mode of the cavity with R=-075*mm* occupies a higher volume at d=0.931m and d=1.862m than the other sets. The resonator with R=-100*mm* provides the lowest volume at 0.931m, the set-up with R=-200*mm* establishes the lowest volume at d=1.862m. The minimum of the volume is found to be at d=2.5m for R=-200*mm*. Mirrors between [-200,-100]*mm* would provide a minimum at d=0.931m and d=1.862m . The influence of the radius of curvature will therefore be considered in the next subsection.

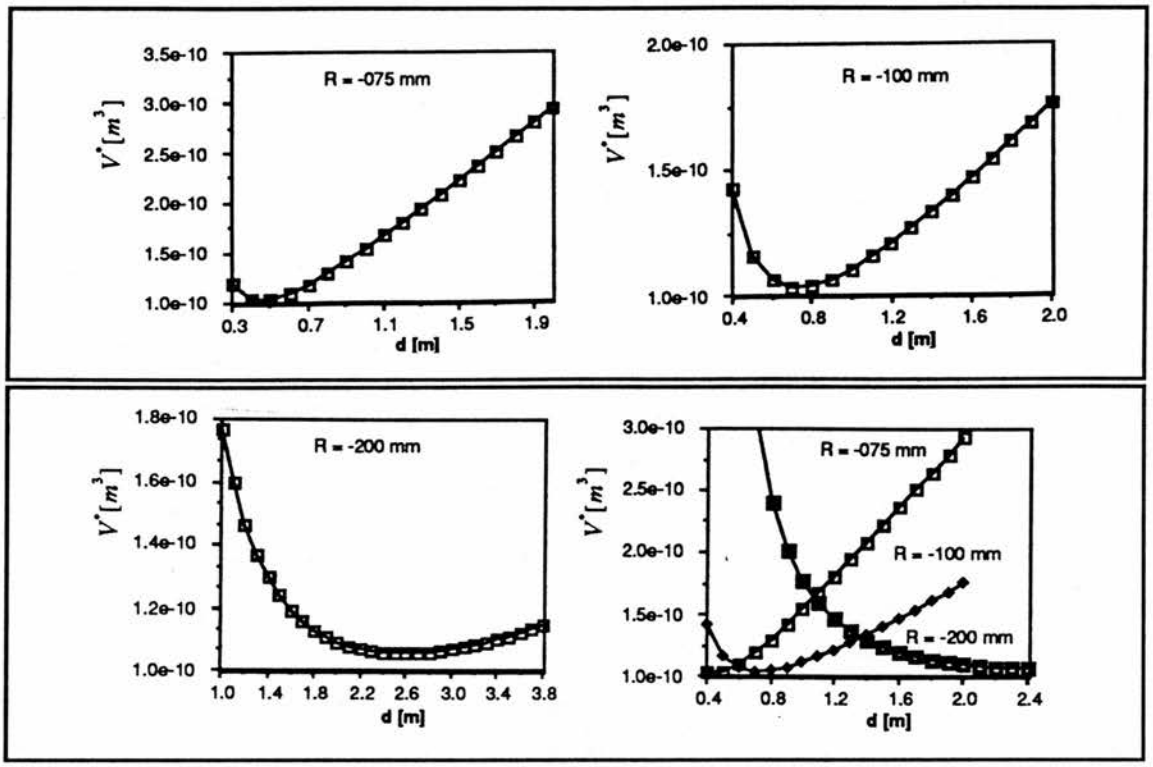

Figure 4.15 : Plot of the volume of the signal inside the rod as a function of the total length of the cavity *d* for all given sets of mirrors R=-075*mm*, R=-100*mm* and R=-200*mm*.

4.2.1.3 Dependence on R

In figure 4.10, 4.11 and 4.16 it can be seen that the stability-ranges $|S_{t,s}|$ increase the larger the absolute value of R becomes. This is due to the fact that the beamwaist for R=-200*mm* is larger than the one for R=-075*mm* and therefore astigmatism is more likely to be found in systems where the beamwaist appears to be smaller. The behaviour of the beamwaist within the crystal is shown in figure 4.14 for R=-100*mm* and R=-200*mm*. Note the much less tightly focused beam in the case of the R=-200*mm* mirrors.

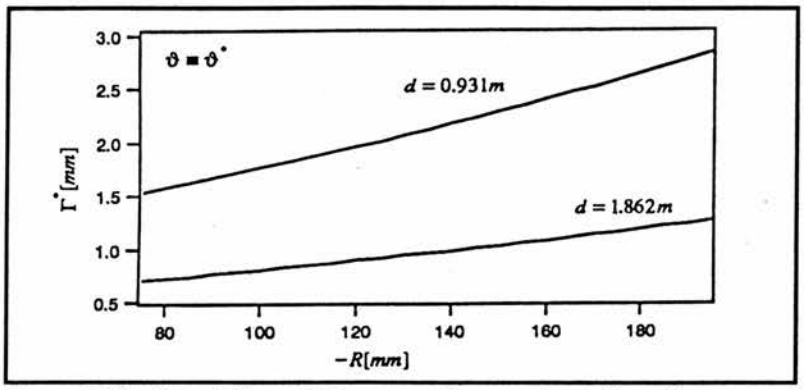

Figure 4.16 : Plot of the stability range Γ versus the radius of curvature R for two fixed lengths of the cavity d=1.862m and d=0.931m. Note that the stability range becomes larger the higher the radius of curvature is chosen and the shorter the cavity is.

In order to minimise the volume of the signal within the rod, the parameter R can also be varied to provide significant change in the volume. For a fixed length of d=1.862m the minimum volume is established - optimum astigmatic compensation provided - at $R \approx -170mm$ whereas for the half length of d=0.931m the optimum R is found with $R \approx -115mm$. This is shown in figure 4.17.

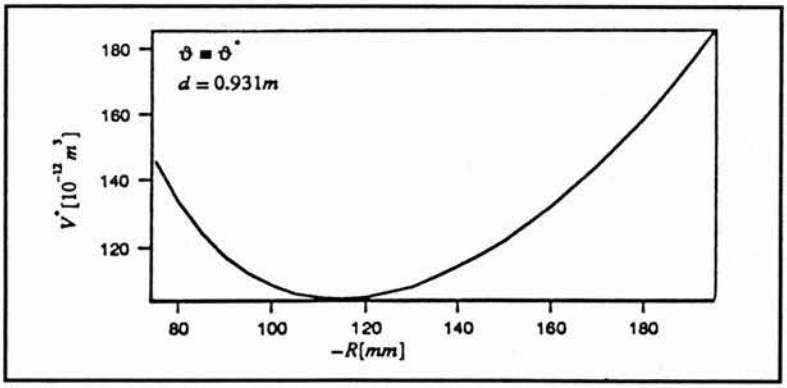

Figure 4.17[a] : The volume inside the crystal is also a critical function of R as long as the length of the cavity d is fixed. This is a plot of the volume V as a function of the radius of curvature R for d=0.931m.

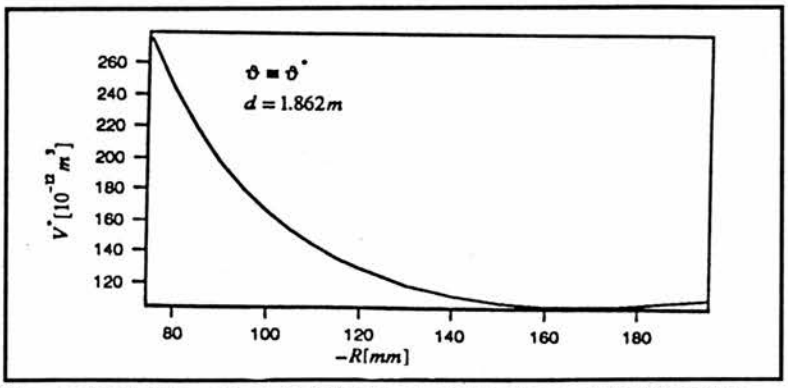

Figure 4.17 : The volume inside the crystal is also a critical function of R as long as the length of the cavity *d* is fixed. This is a plot of the volume *V* as a function of the radius of curvature R for d=1.862m.

Therefore with the R=-200mm mirrors a better performance of the laser at d=1.862m can be expected as well as the R=-100mm mirrors are expected to provide better results at d=0.931m.

4.2.2 Experimental Results

To find the most suitable and efficient laser configuration all different symmetrical mirror sets were used. This means that with pre-focal focusing lenses of f=50mm, 75mm, 100mm, 150mm and 200mm the mirrors of the folding section were chosen to be R=-75mm, -100mm and -200mm. This led to 12 different data sets due to the fact that the distance between crystal and mirror of the folding section limits the applicability of the lenses as $\lambda_{pump} < \lambda_{signal}$ (see figure 3.13). In all these 12 configurations a 1% output coupler was used to ensure low threshold for laser operation. In all set-ups the resonator was constructed using the astigmatic compensation angle ϑ^* and then the length of the resonator was varied by correcting the relative adjustment calculated above in the folding section to δ^* . The pump power was kept constant at 5.2W and the temperature of the crystal was maintained between $8C^o$ and $12C^o$.

The first step was to find the maximum transmission of the pump through the first mirror of the folding section and the crystal by changing the position of the pre-focal lens which means varying the distance defined in chapter 3 of the pre-focal lens to the crystal Δ (see figure 3.13). Having found the optimum Δ, it was kept more or less fixed throughout the whole set-up for a specific mirror set. Parameters varied were the length d of the cavity and the angle ϑ .

The experiment was undertaken with the different pre-focal lenses described above, and the other criteria of efficiency used was to minimise the volume of the pump beam inside the crystal as well as the volume of the signal beam. Therefore the volume of the pump beam was also computed and the minimum volume was found to be achieved by using a pre-focal lens of f=10cm out of a set of 5cm, 7.5cm, 10cm, 15cm and 20cm. The computation included the different mirrors between the lens and the crystal as well as the for a certain length of the cavity required relative adjustment δ^*.

Experimentally for each configuration, the output power was measured as a function of the length of the cavity. A power meter (*Photon Control* model 11SC)was used. For this purpose care was taken to ensure that the optimum alignment was achieved in each configuration. Errors were estimated from fluctuations in the reading of the power meter. These fluctuations are mainly due to fluctuations of the Nd:YAG laser which was used as pump source. The results are shown in figure 4.18.

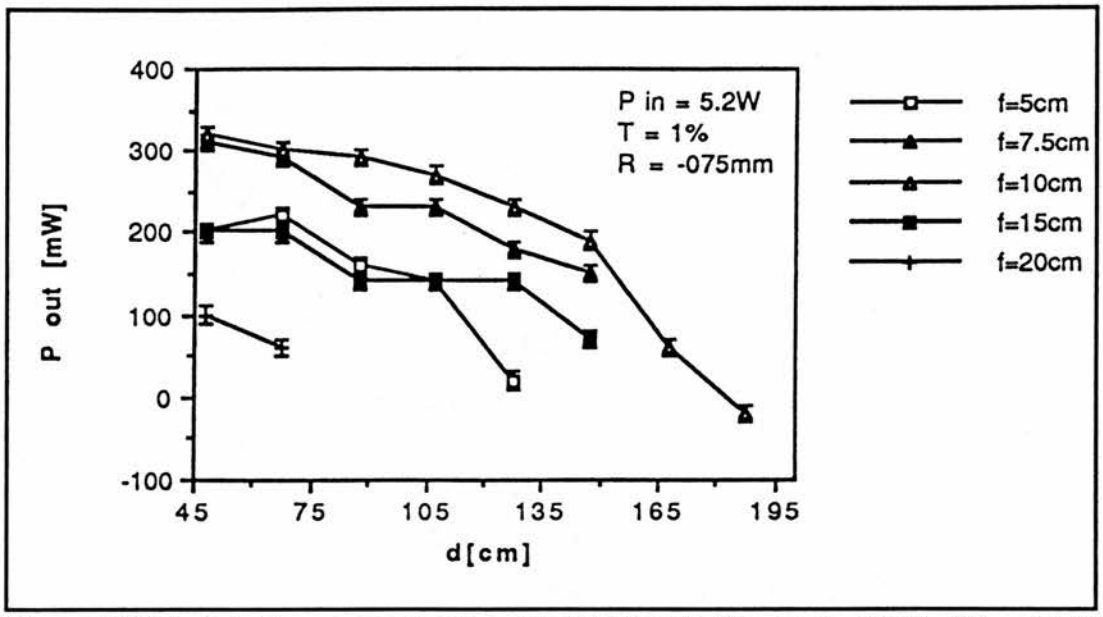

Figure 4.18 [a] : Output power as a function of the total length of the cavity *d* for R=-75*mm* for all given pre-focal lenses.

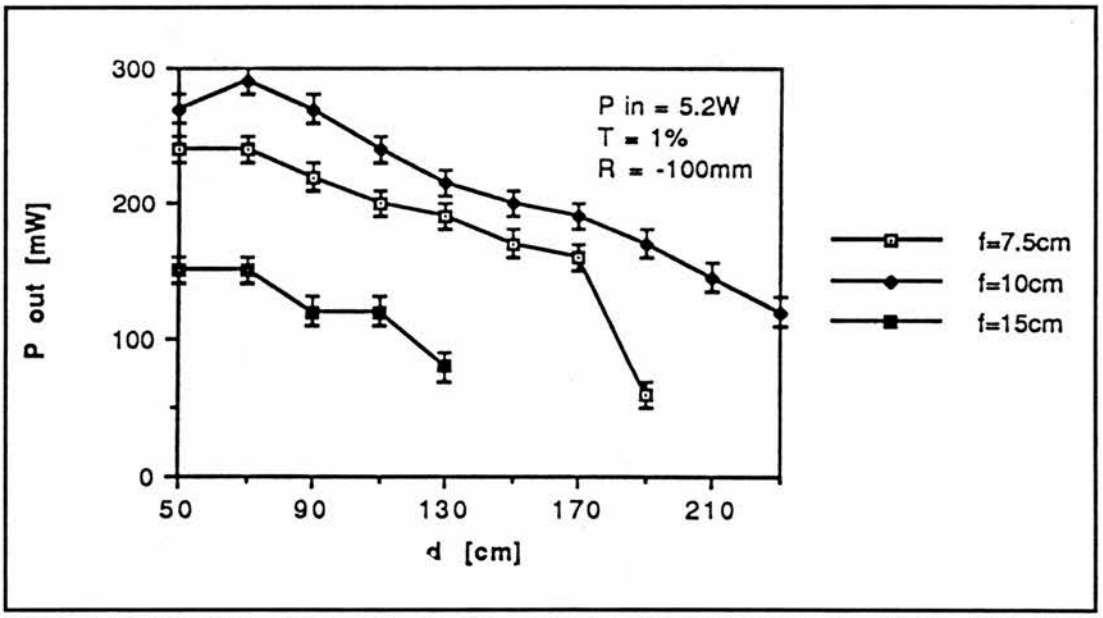

Figure 4.18 [b] : Output power as a function of the total length of the cavity *d* for R=-100*mm* for all given pre-focal lenses.

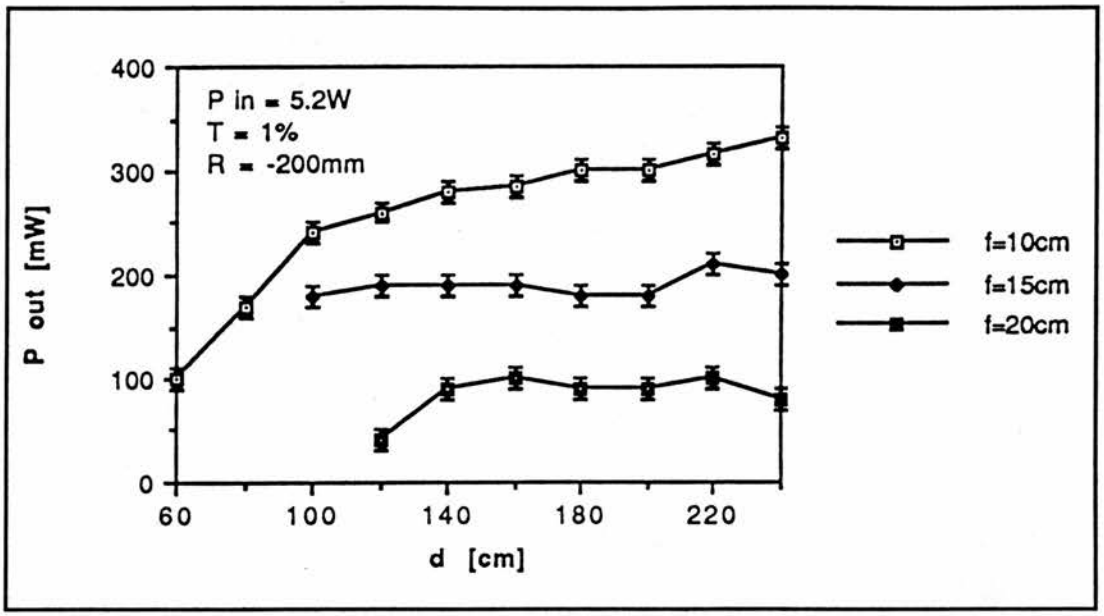

Figure 4.18 [c] : Output power as a function of the total length of the cavity *d* for R=-200*mm* for all given pre-focal lenses.

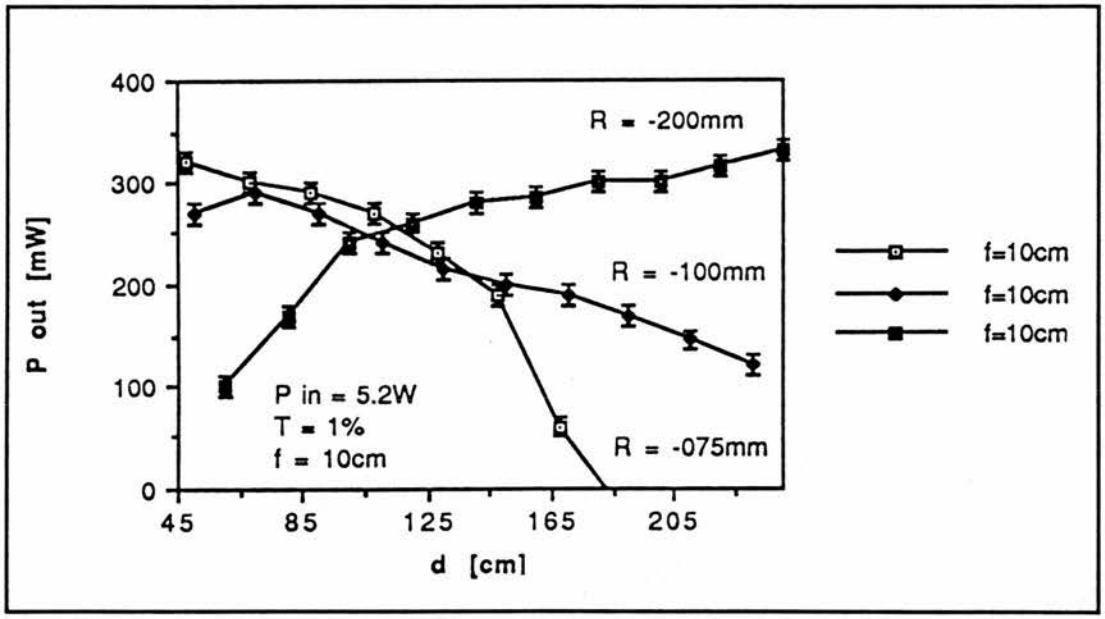

Figure 4.18[d]: Experimental plots of the output power as a function of the total length of the cavity *d* for all given sets of mirrors R=-075*mm*, R=-100*mm* and R=-200*mm* for the pre-focal lens *f*=10*cm*. The transmission of the output coupler is*T*=1% for all measurements. The pump power is 5.2W.

For all three mirror sets it was found that oscillation could only take place in certain ranges of the total length of the cavity *d*. These ranges were the same than the ranges of *d*

found by choosing the volume of the signal being smaller than a fixed volume $\overline{V} = 2.5E-10m^3$only. The performance of the laser was found to be more efficient for a smaller volume of the signal beam. This can be seen by comparing figure 4.15 to figure 4.18[d] and it is in agreement with [Digonnet 1985][8].

On the other hand the choice of the pre-focal lens was found to be crucial as well. The lenses with $f<10cm$ showed too much divergence towards the edges of the crystal and so the volume was too high and the area too small for sufficient pump density to be achieved. The pre-focal lenses with $f>10cm$ were providing soft focusing so that even with the less tightly focused beam they could not provide a smaller volume and so intensity of the pump inside the crystal was not higher than with the lens with $f=10cm$. Therefore the pump density was at its highest at $f=10cm$.The results for $f=10cm$ are shown in figure 4.18-d.

The experiment shows the highest output power for all different mirror sets to be achieved with the pre-focal lens of $f=10cm$. The individual maximum of the output is found to be the configuration for which each set provides a minimum in the volume of the signal inside the rod. This configuration is - ϑ^* provided - only achieved for a certain total length of the cavity d.

The most efficient set-up for $d=1.862m$ was therefore found to be the astigmatically-compensated R=-200mm set (P_{out}=320mW @T=1%), whereas the best lasing-performance at a length of $d=0.931m$ was achieved with the compensated R=-100mm mirror-set ($P_{out}=260mW$ @ T=1%). The optimum P_{out} for the different radius of curvature are listed in table 4.2

R [*mm*]	*d* [*m*]	P_{out} [*mW*]
-075	0.55	310
-100	0.70	290
-200	2.40	340

Table 4.2 : The highest output power for each mirror set and the corresponding length with an output coupler of *T*=1% and pump power of 5.2W.

4.4. Characterisation of Laser Oscillation

The condition to reach threshold or to maintain this level is that the losses within the medium α due to scattering are small enough to allow the net round-trip gain inside the cavity including the mirror reflections to be unity. It is only then that the intensity factor of this threshold provides a wave making a complete round-trip inside the resonator and coming back with the same intensity, and modulo 2π with the same phase shift. The condition of oscillation[9] is:

$$re^{-2i[k+\Delta k(\omega)]l}e^{[\gamma(\omega)-\alpha]l}=1 \qquad (4.1)$$

$r=\prod_n r_i$ where r_i are the different reflection constants of the n mirrors employed in the cavity, $\gamma(\nu)\equiv(N_2-N_1)\frac{c^2}{8\pi n^2\nu^2 t_{spont}}g(\nu)$ is the small signal gain and $g(\nu)$ represents the gain line shape which is derived from the complex susceptibility[10] such that

$$\gamma_t(\omega)=\alpha-\frac{1}{l}\ln(r) \qquad (4.2a)$$

and

$$2[k+\Delta k(\omega)]l=2\pi m \text{ with } m=1,2,3,... \qquad (4.2b)$$

The threshold for the population inversion therefore becomes

$$N_t \equiv (N_2 - N_1)_t = \frac{8\pi n^2 t_{spont}}{g(\nu)\lambda^2}\left(\alpha - \frac{1}{l}\ln(r)\right) \qquad (4.3)$$

4.4.1 Output Power

With expression (4.3) it can be expected that for a pump intensity which causes a higher inversion than N_t the laser will start to oscillate. The relation between emitted power P_e and the effective pumping rate R_{eff} is given by

$$P_e = P_s\left(\frac{R_{eff}}{R_t} - 1\right) \qquad (4.4.)$$

with P_s being the spontaneous emission at threshold and R_t being the pump rate at the threshold.

The relationship between P_e and R_{eff} is therefore a linear one and was experimentally tested. The attenuation of the pump beam was achieved by using a Brewster-wedge attenuator. Care was taken to ensure that the alignment for each measurement was optimised. The results are shown in figure4.19.

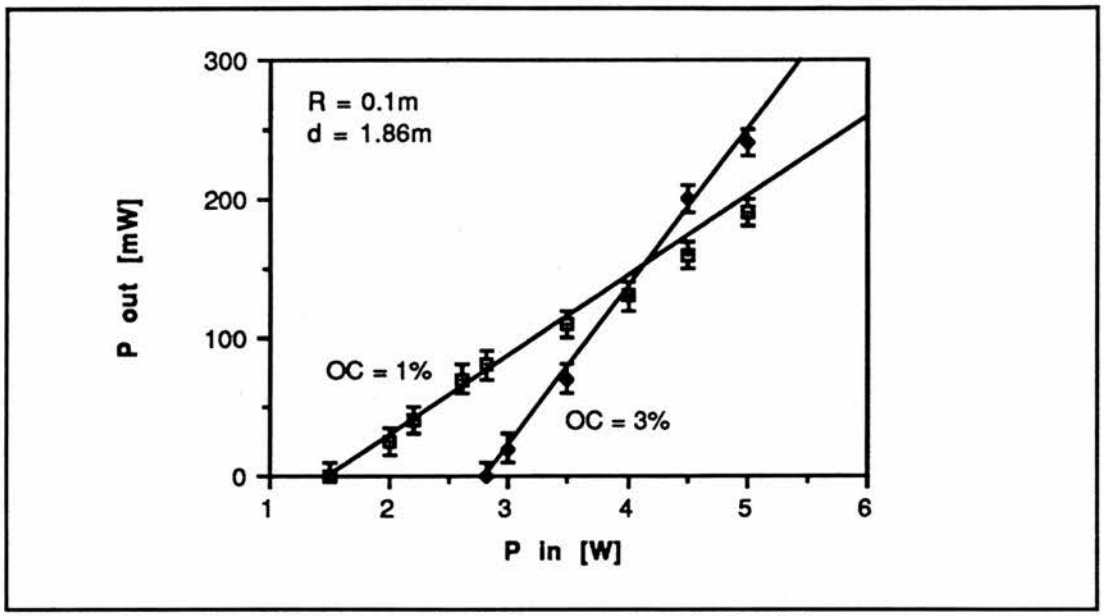

Figure 4.19 [a] : The efficiency curve for the laser operating with R=-100*mm*

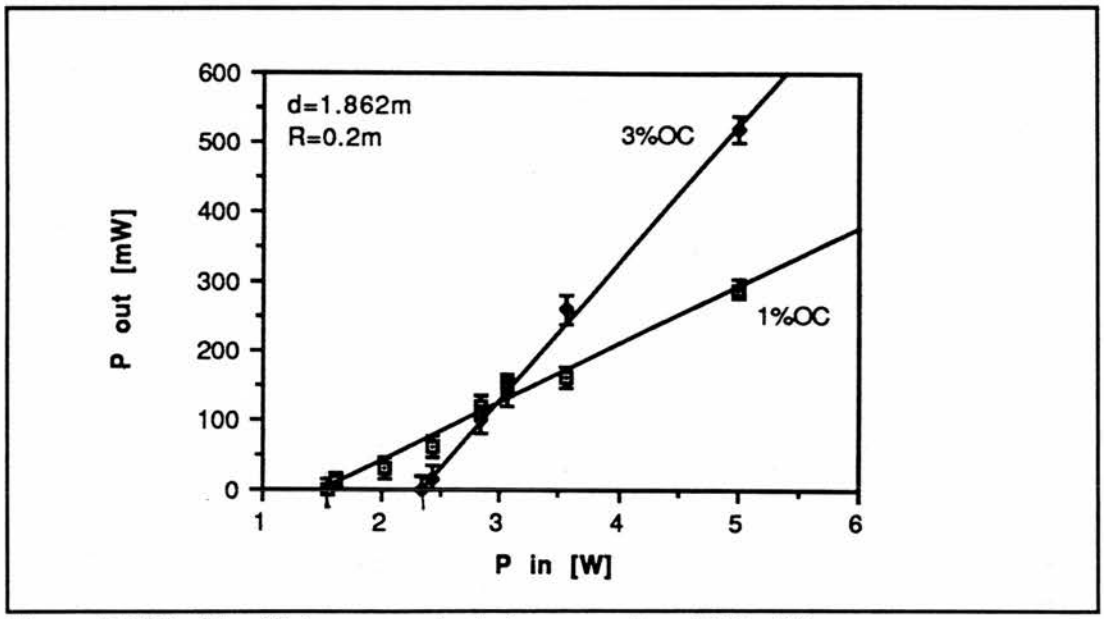

Figure 4.19 [b] : The efficiency curve for the laser operating with R=-200*mm*

The higher the chosen transmission T of the output coupler, the lower the threshold of the system becomes. The efficiency of the different slopes are shown in table 4.3. Higher efficiencies can be achieved by employing the optimum transmission T of the output coupler which will be discussed in section 4.4.3.

R [*mm*]	*T* [%]	P_{th} [*mW*]	P_e/P_{pump}
-200	1	1.53	0.058
-200	3	2.34	0.104
-100	1	1.5	0.038
-100	3	2.8	.048

Table 4.3 : The efficiency values for the curves given in figure 4.19.

4.4.2 Dependence on the Temperature

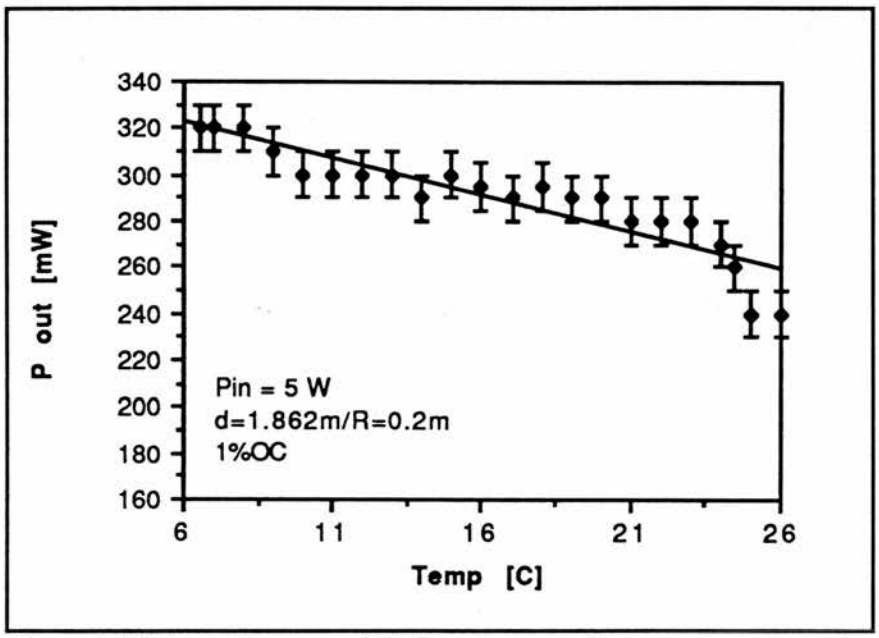

Figure 4.20: The performance of the laser in terms of output power versus the temperature monitored at the crystal.

Temperature control is important in order to avoid thermal lensing of the cavity which decreases the cavity stability. Therefore experiments were also carried out to investigate whether or not the temperature of the crystal influences the performance of the laser. The minimum applicable temperature was limited by the fact that moisture appeared on the surfaces of the crystal at $5°C$ whereas the upper limit has been chosen to be $25°C$

because of the concern about possible thermal damage. The curve is shown in figure 4.20 and the output power drops from 7°C to 20°C by 15% of its value @7°C.

4.4.3 Optimum Output Coupling

The total loss within the cavity can be attributed to the residual losses due to scattering, absorption within the gain medium and the optical elements of the cavity and the useful loss of the coupling of output power through the partially transparent mirror referred to as output coupler. The first losses are the inevitable L_i, the second losses the desired transmission T. The total loss L is therefore

$$L = L_i + T. \qquad (4.5)$$

As L_i does not contribute to the available output power it should be made as small as possible by careful choice and adjustment of the resonator components. In the case of zero output coupling (T=0) the lowest threshold is achieved and the internal circulating intensity is strongest but the available output power is zero. Increasing the loss T leads to more output power but on the other hand to more total loss L as well. Increasing T over a certain limit will lead to an increase of threshold and therefore make oscillating impossible at one stage. This is the maximum allowable output coupling T_{max} beyond which the cavity is overcoupled, so that the total cavity losses L exceed the available gain, and no oscillation is possible. The optimum value for T is found between these two extremes and is given by[11]:

$$T_{opt} = -L_i + \sqrt{g_o L_i} \qquad (4.6)$$

where $g_o = \gamma_o d_{rod}$ is the unsaturated gain per pass. This T_{opt} gives the maximum output power in respect to the established loss due to the output coupler.

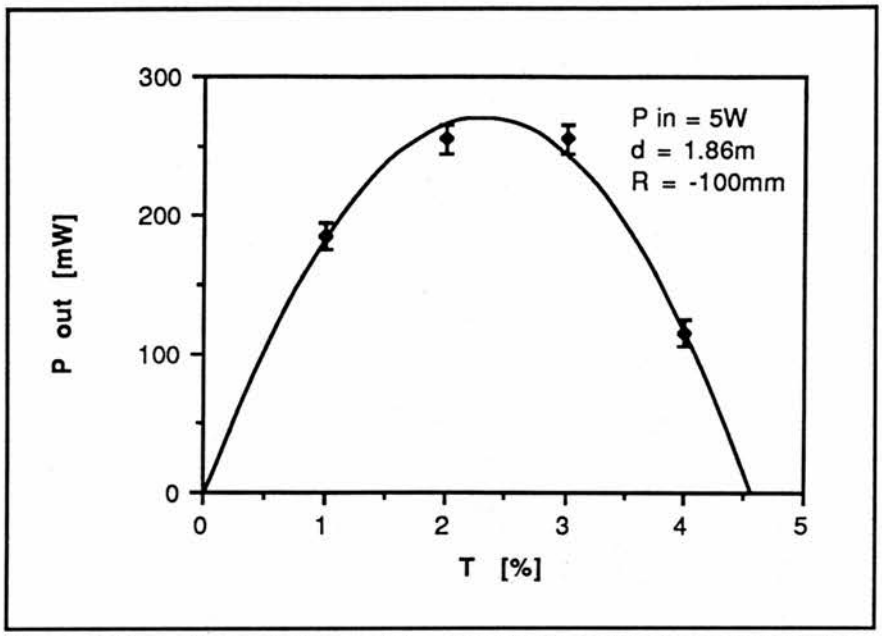

Figure 4.21[a] : The output power P_{out} as a function of the transmission of the output coupler T for R=-100*mm*. The best fit is a polynomial fit of the second order.

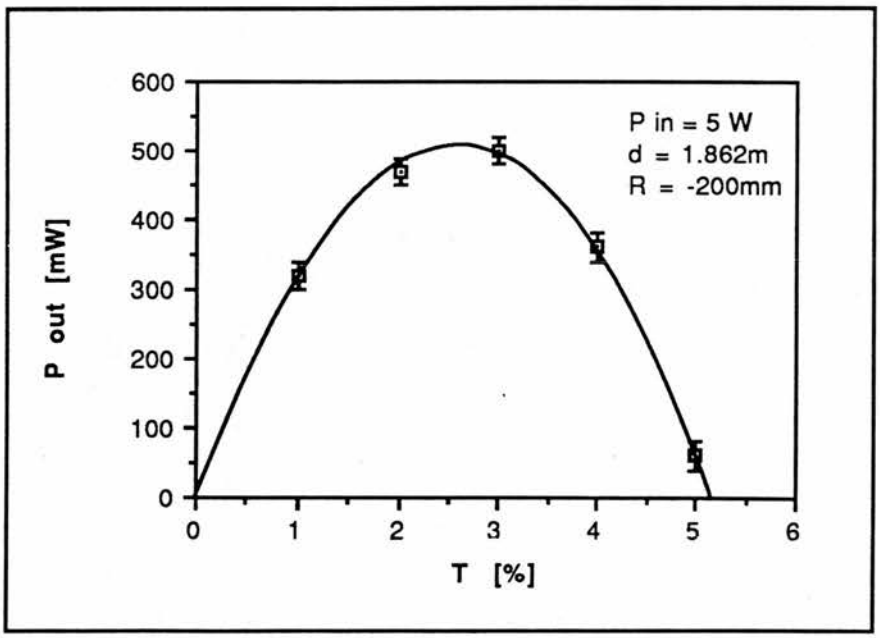

Figure 4.21[b] : The output power P_{out} as a function of the transmission of the output coupler T for R=-200*mm*. The best fit is a polynomial fit of the second order.

The experimentally deduced gradients are given in figure 4.21. For the sets of R=-100mm and R=-200mm the output power P_{out} was plotted as a function of the transmission of the output coupler T.

The curves of figure 4.21 indeed exhibit behaviour qualitatively similar to that expected from the preceding discussion. But note that no attempt has been made to carry out a quantitative comparison with the theory.

4.4.4 Oscillation Frequency

The oscillation frequency of a laser is determined by two factors: From equation 4.2.a given the frequencies at which there is optical gain; and equation 4.2.b which constrains the oscillation frequencies to a discrete number of longitudinal modes. The combination of these two effects gives the frequency that oscillates and to be:

$$\nu = \nu_m - (\nu_m - \nu_o)\frac{\gamma(\nu_m)c}{2\pi n\Delta\nu} \qquad (4.7)$$

with $\nu_m = \frac{mc}{2nd}$ corresponding to the m -th resonance frequency of the passive resonator and ν_o being the centre frequency of the atomic line shape function. In an ideally homogeneously broadened laser, only this mode will oscillate because of preferential gain at its wavelength as soon as the threshold population is exceeded. Most common lasers are limited to sharply defined frequencies of operation that depend on the transitions of the specific atoms employed in the laser, and to fairly narrow tuning ranges that depend on the line widths of these atomic transitions.

4.4.5 Tunability

In Cr^{4+}:*YAG* the fluorescence spectrum is fairly flat over a broad range and the selection of the oscillating mode depends on the inevitable loss $L_i(\nu_m)$ which is related to the mirror reflectivity spectral characteristics or whatever tuning elements are present in the cavity. In the absence of a tuning element such as a prism or a birefringent filter (BRF), the laser still oscillates over a narrow bandwidth, but the wavelength here is a critical function of the laser alignment. The wavelength which oscillates will be that which undergoes minimum overall losses. In this case these are the losses at the Brewster-angled surfaces of the crystal, in the crystal and on the mirrors. In figure 4.22 can be seen that the influence of different mirrors leads to different oscillating wavelengths due to the fact that these mirrors have got slightly different reflection losses for the same wavelengths and the alignment of the laser had to be corrected between these two measurements. Whereas the mirrors with R=-100*mm* lead to oscillation at 1433.5*nm*, the cavity set up with R=-200*mm* produces an output at 1449*nm*.

It is important to consider carefully the frequencies of oscillation of a homogeneously broadened laser. In an ideal homogeneously broadened laser only one mode will oscillate (and it will be the one closest to the line centre), but spatial hole burning generally results in the oscillation of several modes close to line centre. The introduction of a tuning element such as a prism or a thin birefringent filter only allows tuning of the peak wavelength of oscillation of the laser and does not constrain the number of modes that oscillate. The laser therefore oscillates with broad tunability over the fluorescence range but with low spectral purity. In order to improve the spectral purity of the laser output, it is necessary to introduce mode-selecting elements into the cavity such as an etalon. An etalon constrains the laser to oscillate in only one longitudinal mode. This was not done in this work.

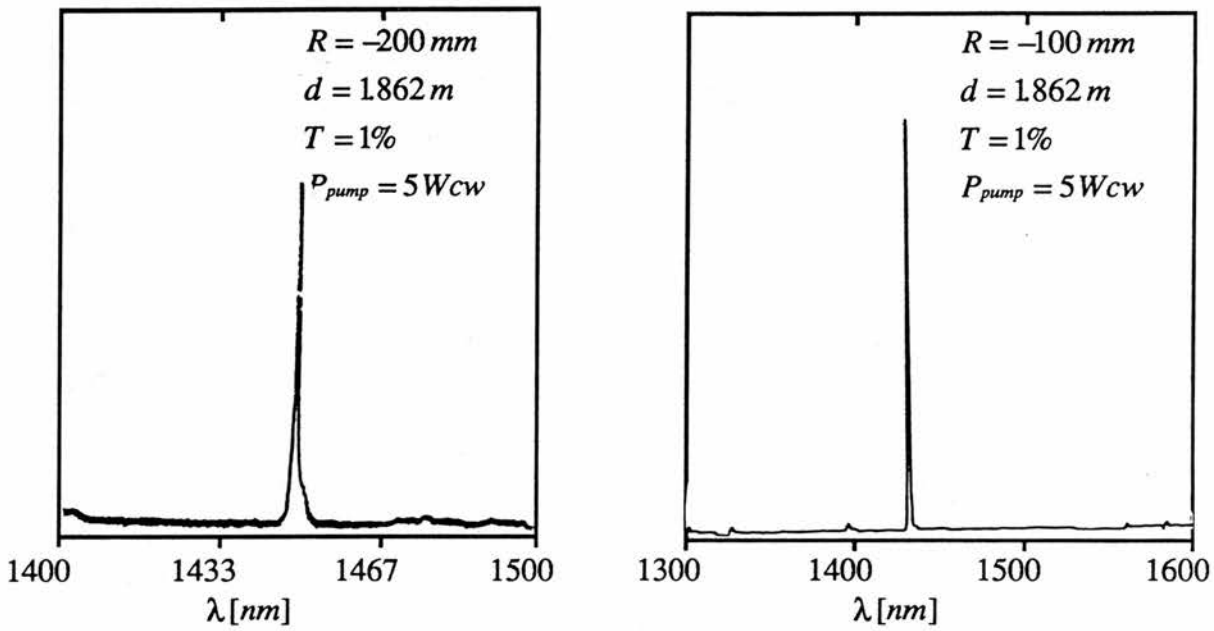

Figure 4.22 : The laser emits power at different wavelength even in absence of tuning elements for different mirrors and a different alignment.

In the experiments to date a 1.6*mm* thick BRF was used and this was incorporated into the arm of the cavity near to the 100% end mirror. Note the slight reduction in the output power with the BRF inserted compared to the output power without the BRF. As the system is homogeneously broadened it is the center wavelength alone which is ideally supposed to oscillate Tuning the peak wavelength to the wavelength in which the laser preferably operates therefore results in nearly the same output power at this wavelength.

The tuning range of 1360*nm* to 1530*nm* measured for a pump power of 5.2W can be seen in figure 4.23 for an output coupler of transmission of T=1%. Note that it is different from the tuning range of [Shestakov 1991] as it lacks the significant drop of power in the region of 1420*nm* to 1500*nm*. Another difference is the slightly broader tuning range of [Shestakov 1991] which probably results from harder pumping causing the threshold for the frequencies at the edge of the tuning curve to be exceeded as well.

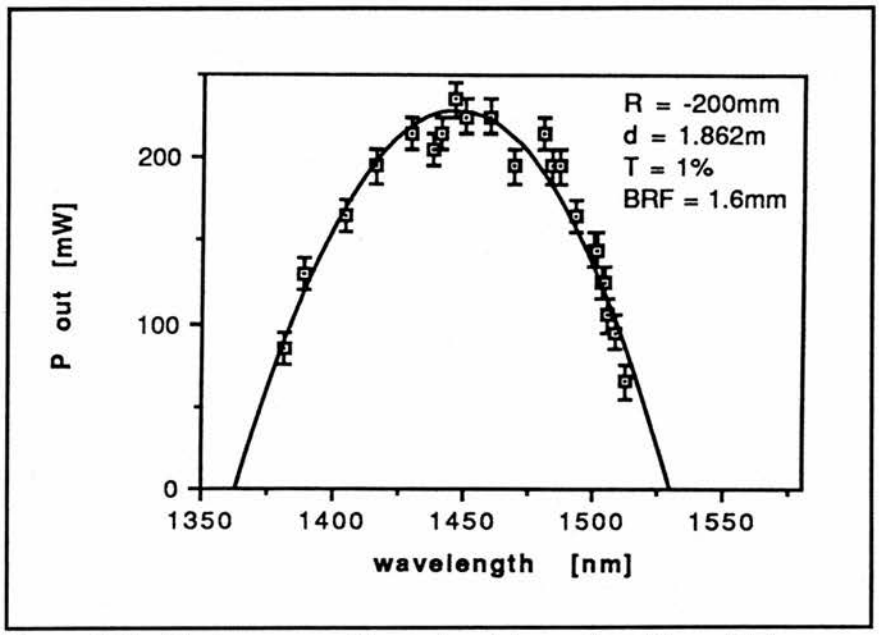

Figure 4.23 : Tuning curve of the system taken with a 1.6*mm* thick BRF.

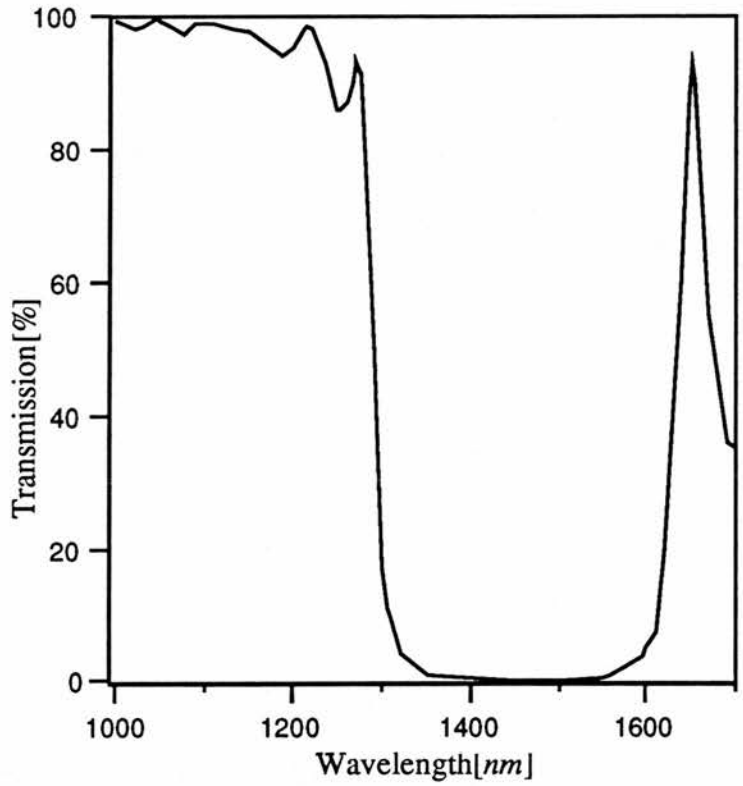

Figure 4.21 : Transmission curve of the mirrors used for the experiments. Note the significant change in the region of 1300*nm* to 1350*nm* and of 1530*nm* to 1650*nm*. The data were supplied by Laseroptik GmbH.

Another reason for this difference is the coating of the mirrors used. The mirrors lose the ability to reflect in the region of 1300*nm* to 1350*nm* and in the region of 1500*nm* to 1600*nm* completely (compare figure 4.21). The performance of the laser with the centre wavelength of 1450*nm* and this tuning curve is obviously determined by the reflectivity of the mirrors. The behaviour found by Borodin and Shestakov[12] can not be seen with these mirrors. The maximum output power was found to be at 1450*nm* for this Cr^{4+}:*YAG*-laser and the useful tuning range is 1360*nm* to 1530*nm*.

4.5 Conclusions

In this chapter the experimental performance of the Cr^{4+}:*YAG* laser has been described. The laser was examined in cw-operation and it was found that its performance was in general agreement with theoretical expectations of [Digonnet 1985][13]. The output power was higher for smaller volumes taken up by signal and pump beams within the crystal. The efficiency of the laser was found to be over 10% and its tuning range was demonstrated to be 1360*nm* to 1530*nm*. In the next chapter preliminary mode-locking studies of this laser will be described.

4.6 References

1 Shestakov A.V. & al.: Tunable Cr^{4+}:*YAG* Lasers, *Conference on Lasers and Electro Optics,* CLEO Baltimore, Marryland, May 12-17 **1991**, Postdeadline-papers

2 Geusic, J.E. & al.: Appl. Phys. Letters, vol.4, p.182, **1964** ; Kushida, T. & al.: Phys.Rev., vol.167, p.1289, **1968**; Koningstein, J.A. & Geusic, J.E.: Pys.Rev., vol. 136, p.711, **1964**

3 Kushida, T. & al.: Phys.Rev., vol.167, p.1289, **1968**

4 Digonnet, M.J.F. & Gaeta, C.J.: *Applied Optics,* Vol24, No.3, p.333, **1985**

5 Kogelnik, H. & al.: *IEEE J.of Qantum Electronics,* vol. QE-8, No.3, p.373, **1972**

6 Kogelnik, H. & al.: *IEEE J.of Qantum Electronics,* vol. QE-8, No.3, p.373, **1972**

7 Hanna, D.C.: *IEEE J. of Quantum Electronics,* vol. QE-5, No.10, p.483, **1969;** Kogelnik, H. & al.: *IEEE J.of Qantum Electronics,* vol. QE-8, No.3, p.373, **1972**

8 Digonnet, M.J.F. & Gaeta, C.J.: *Applied Optics,* Vol24, No.3, p.333, **1985**

9 Siegman, A.E.: Lasers, Mill Valley, California **1986**; Schawlow, A.L. & Townes, C.H.: *Phys.Rev.*, vol.112, p.1940, **1958**

10 Yariv, A.: Optical Electronics, Third Edition, Japan **1985**; Siegman, A.E.: Lasers, Mill Valley, California **1986**

11 Siegman, A.E.: Lasers, Mill Valley, California **1986**; Yariv, A.: Optical Electronics, Third Edition, Japan **1985**

12 Borodin & Shestakov, Izvestiya Akademii Nauk SSSR, Seriya Fizicheskaya, vol.54, No.8, p1500, **1990**

13 Digonnet, M.J.F. & Gaeta, C.J.: *Applied Optics*, Vol24, No.3, p.333, **1985**

5 Conclusion and Suggestions for Further Study

5.1 Conclusions

The Cr^{4+}:YAG-laser designed and built during this project has been shown under optimum condition to generate an average output power $\overline{P_{out}}$ of $520mW$ tunable from $1360nm$ to $1530nm$. While this is quite a satisfactory result on its own, further preliminary investigations were carried out in order to study the feasibility of the system as a mode-locked laser.

5.2 Preliminary Mode-locked Results

Mode-locking refers to the synchronisation of the phases of the longitudinal modes of the laser to produce a pulsed output. Until recently, this has involved the modulation of the gain or the loss of the laser by using some external source such as an acousto-optic modulator or another mode-locked laser in the case of a synchronous pump.

Recently, the self-modelocking technique was demonstrated in solid-state gain media. This is based on a combination of a Kerr nonlinearity in the gain medium and the group velocity dispersion (GVD) compensation.

This was first observed in the J F Allen Physics Research Laboratories in the University of St Andrews for a titanium-sapphire laser and later for a Cr:LiSAF system. It is hoped to extend the technique to the Cr^{4+}:YAG laser. Preliminary mode-locking experiments have been carried out with a synchronously pumped configuration where the Nd:YAG laser has been modelocked. The results have been pulses having duration of about $350ps$. Also active mode-locking has been employed by using an regeneratively acousto-optic

modulator. This mode-locker has only arrived recently and best results were achieved by my colleague Dr.Zhu with puls duration as short as 44*ps* (see figure 5.1).

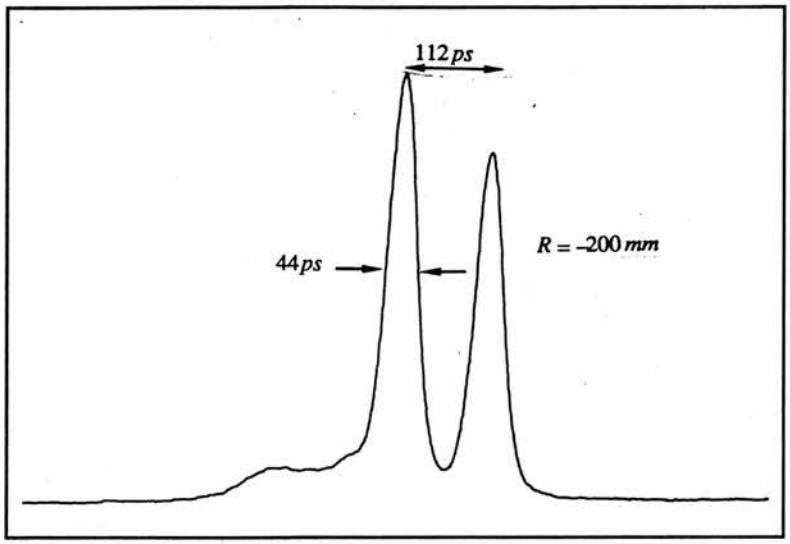

Figure 5.1 : Picosecond pulses observed in the actively mode-locked Cr^{4+}:*YAG*-laser.observed with a streak-camera. The laser was mode-locked by a regeneratively driven acousto-optic mode-locker.

5.3 Suggestions for Further Studies

At this stage, femtosecond pulse generation has not been observed. Reasons for this can be that the operation with the radius of curvature of R=-200*mm* gives optimum cw-performance,but may be that the intensity is insufficient to observe significant Kerr non-linearity. It was also noted, that the cavity configuration used did not compensate for coma. This could cause an non-optimum overlap between pump and signal. Recent reports indicate[1] that stable femtosecond pulses could only be achieved with net negative GVD-compensation[2] . Therefore prisms would be required to be incorporated into the cavity.

Provided the Cr^{4+}:*YAG* laser can be modelocked to produce femtosecond pulses in the 1350-1500*nm* tuning range then this would represent a very convenient near-infrared

ultrashort-pulse source. Its operation in a room-temperature condition makes its convenience rather obvious and its applicability to time-resolved spectroscopy would therefore be assured. Further studies of this laser system are therefore to be greatly welcomed in the future.

5.4 References

1 Knox, W. H., *Optics Letters*, vol.17, No. 7, p.514, **1992**
2 Fork, R.L. & al., *Opt. Letters*, vol.9, p.150 **1984**

Acknowledgements

I wish to thank my supervisor Professor Wilson Sibbett for his support and the opportunity to work on **Cr^{4+}:YAG** in his laboratories. I would also like to acknowledge the work of Dr. Zhu with whom I worked together at this system. I am also grateful to the other members of the W squad because of their unbeatable sense of humour, in particular:

Robert Grant for never laughing but sharing his desk with me

and John McDudley for assisting with Mat-Lab and its 3-D abilities.

bt ar